Article

Molecular Cell

Poly(ADP-Ribose) Prevents Pathological Phase Separation of TDP-43 by Promoting Liquid Demixing and Stress Granule Localization

Graphical Abstract

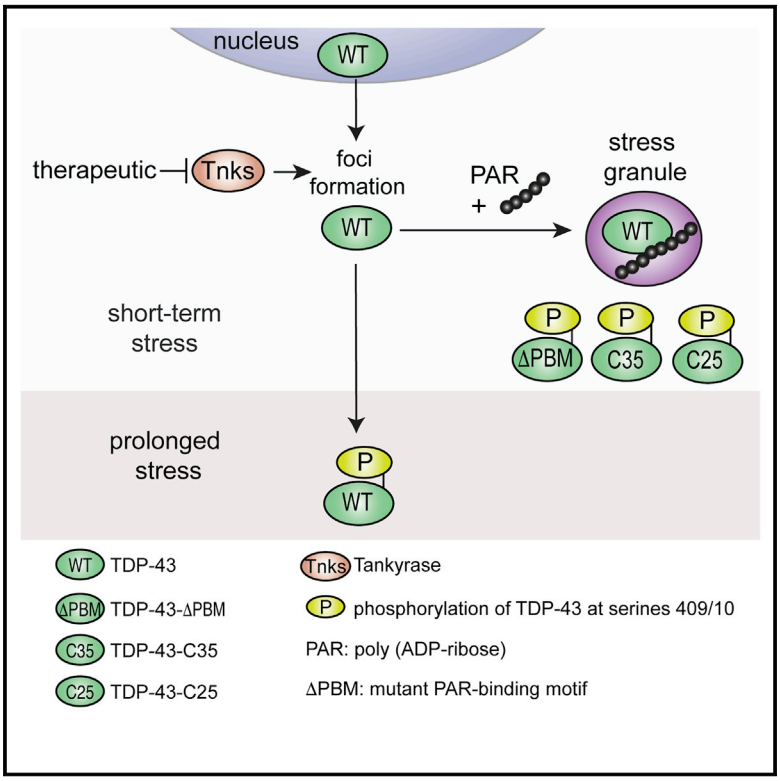

Highlights

- The NLS contains PAR-binding motifs that localize TDP-43 to stress granules
- PAR promotes TDP-43 liquid-liquid phase separation
- Stress granules protect TDP-43 from disease-associated phosphorylation
- Tankyrase regulates cytoplasmic accumulation of TDP-43

Authors

Leeanne McGurk, Edward Gomes, Lin Guo, ..., Robert G. Kalb, James Shorter, Nancy M. Bonini

Correspondence

jshorter@pennmedicine.upenn.edu (J.S.), nbonini@sas.upenn.edu (N.M.B.)

In Brief

McGurk et al. show that TDP-43 is a PAR-binding protein and that this function stimulates liquid-liquid phase separation and stress granule localization. Under short-term stress, the stress granule protects TDP-43 from phosphorylation. TDP-43 foci that persist during long-term stress transition into the phosphorylated state. Inhibition of the PARP Tankyrase mitigates both the cytoplasmic accumulation of TDP-43 and neuronal degeneration.

McGurk et al., 2018, Molecular Cell *71*, 1–15
September 6, 2018
https://doi.org/10.1016/j.molcel.2018.07.002

CellPress

Please cite this article in press as: McGurk et al., Poly(ADP-Ribose) Prevents Pathological Phase Separation of TDP-43 by Promoting Liquid Demixing and Stress Granule Localization, Molecular Cell (2018), https://doi.org/10.1016/j.molcel.2018.07.002

Molecular Cell
Article

Poly(ADP-Ribose) Prevents Pathological Phase Separation of TDP-43 by Promoting Liquid Demixing and Stress Granule Localization

Leeanne McGurk,[1] Edward Gomes,[2] Lin Guo,[2] Jelena Mojsilovic-Petrovic,[3,4] Van Tran,[1] Robert G. Kalb,[3,4] James Shorter,[2,*] and Nancy M. Bonini[1,5,*]
[1]Department of Biology, University of Pennsylvania, Philadelphia, PA 19104, USA
[2]Department of Biochemistry and Biophysics, Perelman School of Medicine at the University of Pennsylvania, Philadelphia, PA 19104, USA
[3]Department of Neurology, Children's Hospital of Philadelphia, Joseph Stokes Jr. Research Institute, Philadelphia, PA 19104, USA
[4]Present address: Les Turner ALS Center at Northwestern Medicine, Feinberg School of Medicine, Northwestern University, Chicago, IL 60611, USA
[5]Lead Contact
*Correspondence: jshorter@pennmedicine.upenn.edu (J.S.), nbonini@sas.upenn.edu (N.M.B.)
https://doi.org/10.1016/j.molcel.2018.07.002

SUMMARY

In amyotrophic lateral sclerosis (ALS) and frontotemporal degeneration (FTD), cytoplasmic aggregates of hyperphosphorylated TDP-43 accumulate and colocalize with some stress granule components, but how pathological TDP-43 aggregation is nucleated remains unknown. In *Drosophila*, we establish that downregulation of *tankyrase*, a poly(ADP-ribose) (PAR) polymerase, reduces TDP-43 accumulation in the cytoplasm and potently mitigates neurodegeneration. We establish that TDP-43 non-covalently binds to PAR via PAR-binding motifs embedded within its nuclear localization sequence. PAR binding promotes liquid-liquid phase separation of TDP-43 *in vitro* and is required for TDP-43 accumulation in stress granules in mammalian cells and neurons. Stress granule localization initially protects TDP-43 from disease-associated phosphorylation, but upon long-term stress, stress granules resolve, leaving behind aggregates of phosphorylated TDP-43. Finally, small-molecule inhibition of Tankyrase-1/2 in mammalian cells inhibits formation of cytoplasmic TDP-43 foci without affecting stress granule assembly. Thus, Tankyrase inhibition antagonizes TDP-43-associated pathology and neurodegeneration and could have therapeutic utility for ALS and FTD.

INTRODUCTION

In almost all cases of amyotrophic lateral sclerosis (ALS) and ~50% of frontotemporal degeneration (FTD), the normally nuclear RNA-binding protein transactive response (TAR) DNA binding protein of 43 kDa (TDP-43) forms phosphorylated aggregates in the cytoplasm of affected neurons and glia (Hasegawa et al., 2008; Mackenzie et al., 2007; Neumann et al., 2006). Increasing evidence suggests that stress pathways are central to ALS and FTD, collectively known as ALS/FTD. For example, TDP-43, along with other RNA-binding proteins associated with ALS/FTD, including FUS, Ataxin 2, TIA-1, and hnRNPA1, are components of stress granules (Li et al., 2013). Stress granules are cytoplasmic membraneless organelles that sequester RNA-protein complexes involved in the initiation of protein translation (Kedersha et al., 1999). In *post-mortem* tissue, phosphorylated TDP-43 congregates with the stress granule proteins eIF3, TIA-1, and PABPC-1 (Bentmann et al., 2012; Liu-Yesucevitz et al., 2010; McGurk et al., 2014). In cellular and animal models of ALS and FTD, stress granule biogenesis may also contribute to the degenerative process because downregulation of the stress granule proteins Ataxin-2 and poly(A)-binding protein (PABP) mitigates disease-associated toxicity (Becker et al., 2017; Elden et al., 2010; Kim et al., 2014; Zhang et al., 2018). Although mounting pathological and genetic evidence implicates stress pathways in ALS and FTD, how stress contributes to disease and to TDP-43-associated pathology remains enigmatic.

Stress granule assembly occurs via condensation of localized RNA-protein complexes into dynamic liquid droplets—a process called liquid-liquid phase separation (LLPS) (Hyman et al., 2014; Wippich et al., 2013). A remarkable feature of proteins that localize to stress granules is that they can undergo spontaneous LLPS *in vitro* (Lin et al., 2015; Mackenzie et al., 2017; Molliex et al., 2015; Murakami et al., 2015; Patel et al., 2015). Protein domains important for LLPS tend to be intrinsically disordered regions, including the prion-like domains (PrLDs) of the ALS-associated proteins hnRNPA1, FUS, TIA1, and TDP-43, which drive LLPS as well as the formation of solid gel-like structures (Conicella et al., 2016; Han et al., 2012; Kato et al., 2012; Lin et al., 2015; Mackenzie et al., 2017; Molliex et al., 2015; Murakami et al., 2015; Patel et al., 2015; Ryan et al., 2018; Sun et al., 2011; Xiang et al., 2015). Although TDP-43 has been shown to phase-separate, it is unknown how LLPS of TDP-43 is regulated in health and disease. Thus, uncovering the regulatory mechanisms that link LLPS, stress granule assembly, and abnormal protein accumulation could illuminate important pathways relevant to disease.

A regulator of protein localization and liquid demixing in the cellular milieu is poly(ADP-ribose) (PAR) (Krietsch et al., 2013; Leung, 2014). PAR is a negatively charged biopolymer that is covalently attached to target proteins by PAR polymerases (PARPs) (Gibson and Kraus, 2012). The PAR polymer is recognized by "reader" proteins, and, in this way, PAR reading drives the assembly of protein complexes (Krietsch et al., 2013; Teloni and Altmeyer, 2016). PARP activity regulates a plethora of cellular processes (Caldecott, 2014; Fatokun et al., 2014; Hottiger, 2015; Hsiao and Smith, 2008), including stress granule assembly (Catara et al., 2017; Isabelle et al., 2012; Leung et al., 2011). Here we demonstrate that reduction of the PARP *tankyrase* inhibits TDP-43-associated neurodegeneration *in vivo*. We show that Tankyrase-1/2 regulates the formation of stress-induced cytoplasmic TDP-43 foci in mammalian cells and that PAR binding to TDP-43 regulates stress granule recruitment. These studies provide insight into the liquid demixing of TDP-43 and suggest that small-molecule inhibitors of Tankyrase could be developed as therapeutic agents for ALS/FTD.

RESULTS

Tankyrase Modulates TDP-43-Associated Toxicity in *Drosophila*

To identify novel pathways relevant to TDP-43-associated toxicity, we initiated a genetic modifier screen in the fly. Selective expression of the human TDP-43 protein in the fly eye using the *glass multiple repeat*-GAL4 (*gmr*-GAL4) driver leads to external and internal degeneration (Figure 1A). In the screen, we discovered that downregulation of *tankyrase* (*Tnks*, CG4719), a PARP (Smith et al., 1998), significantly reduced degeneration of the eye (Figures 1A–1D). We confirmed that expression of the inverted repeat reduced *Tnks* mRNA levels (0.5 ± 0.1 fold ± SEM of normal levels) (Figure S1A) and that reduced *Tnks* had no effect on total TDP-43 protein levels or the levels of a control protein (β-galactosidase) (Figures S1B and S1C), indicating that downregulation of *Tnks* did not affect the GAL4 expression system. Additionally, reduction of *Tnks* had no effect on the Alzheimer's disease- and FTD-associated protein Tau (Figure S1D); thus, the interaction was selective for TDP-43-associated degeneration. Finally, upregulation of *Tnks* enhanced TDP-43-associated toxicity in the eye without having an effect on the eye morphology on its own (Figure S1E) or on the GAL4 expression system (Figure S1F). Together, these data implicate *Tnks* as a novel dose-sensitive regulator of TDP-43-associated degeneration.

We extended these studies to the fly CNS. Neuronal expression of TDP-43 with the *elav*-GAL4 driver resulted in early death (Figure 1E). Downregulation of *Tnks* significantly restored the lifespan defects of the TDP-43 flies while having no effect on the lifespan of controls (Figure 1E; Figures S1G and S1H). Downregulation of *Tnks* in the nervous system had no effect on the total protein levels of TDP-43 (Figures 1F and 1G). However, lowered *Tnks* levels led to a significant increase in nuclear TDP-43 (1.9 ± 0.1 [SEM]) and a significant decrease in cytoplasmic TDP-43 (0.6 ± 0.1 [SEM]) compared with the control (Figures 1F and 1G and S1I and S1J). Taken together, these data indicate that the downregulation of *Tnks* in the nervous system correlates with increased nuclear TDP-43 and mitigates TDP-43-induced degeneration of the nervous system.

TDP-43 Binds to PAR via the Nuclear Localization Sequence

A previous proteomics screen identified TDP-43 as one of many proteins that co-immunoprecipitated with a PAR glycohydrolase (PARG) (Gagné et al., 2012), suggesting that TDP-43 could be a PAR-binding protein. Given that *Tnks* genetically interacted with TDP-43 in the fly, we determined whether TDP-43 and PAR may associate in the same protein complex. Human TDP-43 was expressed in the fly nervous system, and, under non-denaturing conditions, we observed PAR to co-immunoprecipitate with TDP-43 from fly protein lysate (Figure 2A). Furthermore, PAR and endogenous TDP-43 co-immunoprecipitated from mammalian cells (Figures 2B and 2C). These data indicate that TDP-43 and PAR can co-exist in the same protein complex in fly and mammalian protein lysates and raise the possibility that TDP-43 non-covalently interacts with PAR.

To ascertain whether TDP-43 could bind to PAR, we performed a PAR-binding dot blot. Wild-type (WT) TDP-43 (glutathione S-transferase [GST]-TDP-43-WT) was spotted onto a membrane with a canonical PAR-binding protein, histone H4 (Panzeter et al., 1993), and a GST-negative control. Incubation with PAR polymer followed by immunoblotting with an antibody directed to PAR revealed that both histone H4 and TDP-43 bound to PAR (Figure 2D). The most common PAR-binding module is the PAR-binding motif (PBM) (Teloni and Altmeyer, 2016). Alignment of the PBM ($[HKR]_1$-X_2-X_3-$[AIQVY]_4$-$[KR]_5$-$[KR]_6$-$[AILV]_7$-$[FILPV]_8$; Gagné et al., 2008) to TDP-43 revealed that the region with the highest similarity (80%) was in the nuclear localization sequence (NLS) (Figures 2E and S2A); a second site with lower similarity (63%) was also identified within the NLS (Figures 2E and S2A). TDP-43 has a bipartite NLS typified by two clusters of basic amino acids, mutation of which leads to cytoplasmic accumulation of TDP-43 (Winton et al., 2008). Curiously, it was these clusters of basic residues that aligned to the PBM. Here we refer to these two regions as PBM1 and PBM2 (Figure 2E). These data raised the intriguing possibility that the NLS of TDP-43 may be involved in binding to PAR. To verify this possibility, we performed PAR-binding dot blots on peptides that span PBM1 or PBM2 (Figures 2F and 2G). This revealed that PAR bound to the peptide corresponding to PBM2 of TDP-43 (Figure 2G) and not to the peptide corresponding to PBM1 (Figure 2G). These data suggest that the NLS and PBM2 of TDP-43 is a region capable of binding to PAR.

We next determined whether mutation of the PBMs in the full-length TDP-43 protein altered PAR binding and substituted the key lysine and arginine residues with alanine in PBM1, PBM2, or both (ΔPBM). Mutation of PBM1, PBM2, or both led to a significant reduction in PAR binding to TDP-43 (0.23 ± 0.08-fold, 0.11 ± 0.04-fold, and 0.09 ± 0.03-fold ± SEM, respectively, of WT levels) (Figures 2H and 2I). These data indicate that although the PBM2 peptide, but not the PBM1 peptide, can directly bind to PAR, mutation of either PBM is sufficient to diminish the capacity of the full-length protein to bind to PAR. Taken together, these data implicate TDP-43 as a PAR-binding protein and establish the NLS as a region that mediates this interaction.

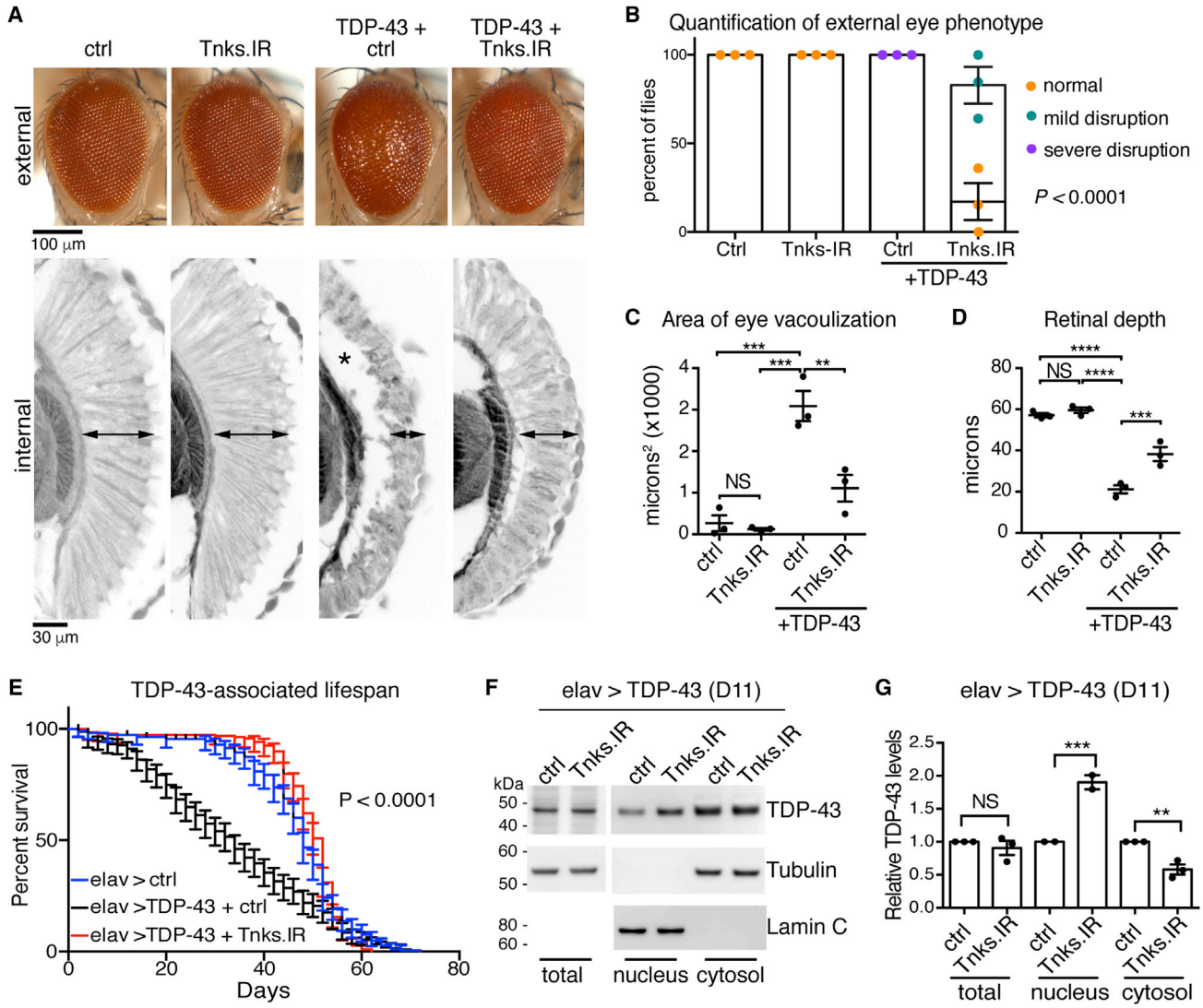

Figure 1. Tankyrase Modulates TDP-43 Toxicity in the Fly

(A) Compared with control (ctrl), human TDP-43 (TDP-43+ ctrl) disrupted the external eye (top panel) and internal retina (bottom panel; arrowheads are retinal width. asterisk is vacuolization). Reduction of *Tnks* (Tnks.IR) mitigates the degeneration of TDP-43 (TDP-43 + Tnks.IR) and has no effect on its own (Tnks.IR).

(B) Reduction of *Tnks* improved the external eye of TDP-43 flies. Mean (± SEM), n = 3, and two-way ANOVA ($p < 0.0001$).

(C) Reduction of *Tnks* reduced vacuolization of the TDP-43 retina. Mean (± SEM), n = 3, one-way ANOVA ($p < 0.0001$), and Tukey's test. Asterisks, significant; NS, not significant.

(D) Reduction of *Tnks* increased the retinal width of TDP-43 flies. Mean (± SEM), n = 3, one-way ANOVA ($p < 0.0001$), and Tukey's test. Asterisks, significant.

(E) Reduction of *Tnks* (Tnks.IR) mitigated the lifespan defect of flies expressing TDP-43 in the brain. More than 190 male flies were followed per genotype. Log rank test for trend, $p < 0.0001$.

(F) Reduction of *Tnks* (Tnks.IR) had no effect on total TDP-43 levels but increased nuclear and decreased cytoplasmic TDP-43.

(G) TDP-43 protein levels relative to control protein (F). Mean (± SEM), one-way ANOVA ($p < 0.001$), and Tukey's test. Asterisks, significant. **$p < 0.01$, ***$p < 0.001$, and ****$p < 0.0001$.

Genotypes are as follows:

In (A)–(D), ctrl (control) is *UAS-mCD8-GFP/+; gmr-GAL4 (III)/+*. Tnks.IR is *UAS-Tnks.IR/+; gmr -GAL4 (III)/+*. TDP-43 + ctrl is *UAS-TDP-43(M)/UAS-mCD8-GFP; gmr-GAL4 (III)/+* and TDP-43+Tnks-IR is *UAS-TDP-43 (M)/UAS-Tnks-IR$^{4179R-4}$; gmr-GAL4 (III)/+*.

In (E)–(G), elav > ctrl (control) is *UAS-mCD8-GFP/+; elav3A-GAL4/+*. elav > TDP-43 + ctrl is *UAS-mCD8-GFP/+; elav3A-GAL4, UAS-TDP-43 (S)/ +* and elav > TDP-43+Tnks.IR is *UAS-Tnks-IR$^{4179R-4}$/+; elav3A-GAL4, UAS-TDP-43 (S)/+*.

See also Figure S1.

PAR Promotes LLPS of TDP-43

PAR seeds protein localization and liquid demixing *in vivo* (Leung, 2014; Teloni and Altmeyer, 2016). Liquid demixing is also an *in vitro* characteristic of proteins associated with ALS (Harrison and Shorter, 2017). Thus, we assessed whether TDP-43 could undergo liquid demixing (LLPS) *in vitro* and whether

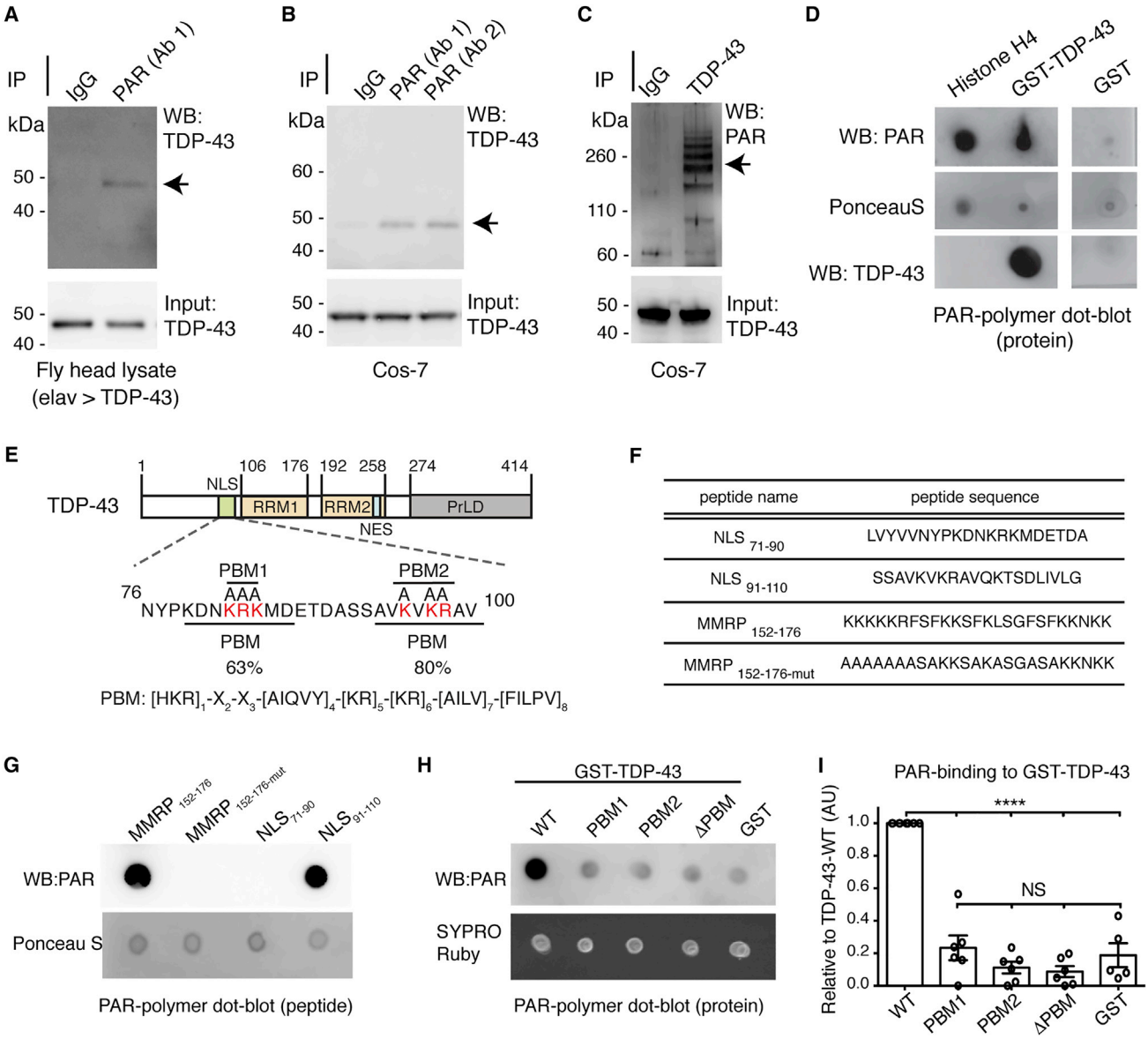

Figure 2. TDP-43 Binds to PAR via a PAR-Binding Region in the N Terminus

(A) Human TDP-43 expressed in the fly brain co-immunoprecipitated with PAR (arrow). PAR antibody: clone 10H, BSA-free, Tulip Biolabs. Head lysate was purified from the adult fly head on day 4. elav > TDP-43 is +/+; *elav3A-GAL4, UAS-TDP-43 (S)/ +*.

(B) PAR from COS-7 cells co-immunoprecipitated with endogenous TDP-43 (arrow). Antibodies: Ab1, anti-PAR, clone 10H, BSA-free, Tulip Biolabs; Ab2, anti-PAR, Enzo Life Sciences.

(C) Endogenous TDP-43 from COS-7 cells co-immunoprecipitated with PAR (arrows). The PAR antibody was LP96 from BD Pharmingen.

(D) GST-TDP-43-WT binds to PAR. Replica membranes were stained for Ponceau S and immunoblotted for TDP-43.

(E) TDP-43 domains. NLS, nuclear localization sequence; RRM, RNA recognition motif; NES, nuclear export sequence; PrLD: prion-like domain. The PAR-binding motifs (PBMs) in the NLS are PBM1 and PBM2. The basic amino acids in PBM1 and PBM2 (red) were mutated to alanine for this study.

(F) Peptides spanned either PBM1 ($NLS_{71–90}$) or PBM2 ($NLS_{91–110}$). MARCKS/MARCKS-related protein (MMRP) amino acids 152–176 ($MMRP_{172–156}$) was the positive control and $MMRP_{152–176\text{-mut}}$ was the negative control (Pleschke et al., 2000).

(G) PAR binding was detected on $MMRP_{152–176}$ and on $NLS_{91–110}$. Replica membranes were stained with Ponceau S.

(H) Mutation of PBM1, PBM2, or both (PBM) in GST-TDP-43 diminished PAR binding. Replica membranes were stained with SYPRO Ruby.

(I) PAR dot blots quantified for PAR immunoreactivity relative to TDP-43. Mean (± SEM), n = 6, one-way ANOVA ($p < 0.0001$), and Tukey's test. Asterisks, significant. ****$p < 0.0001$.

See also Figure S2.

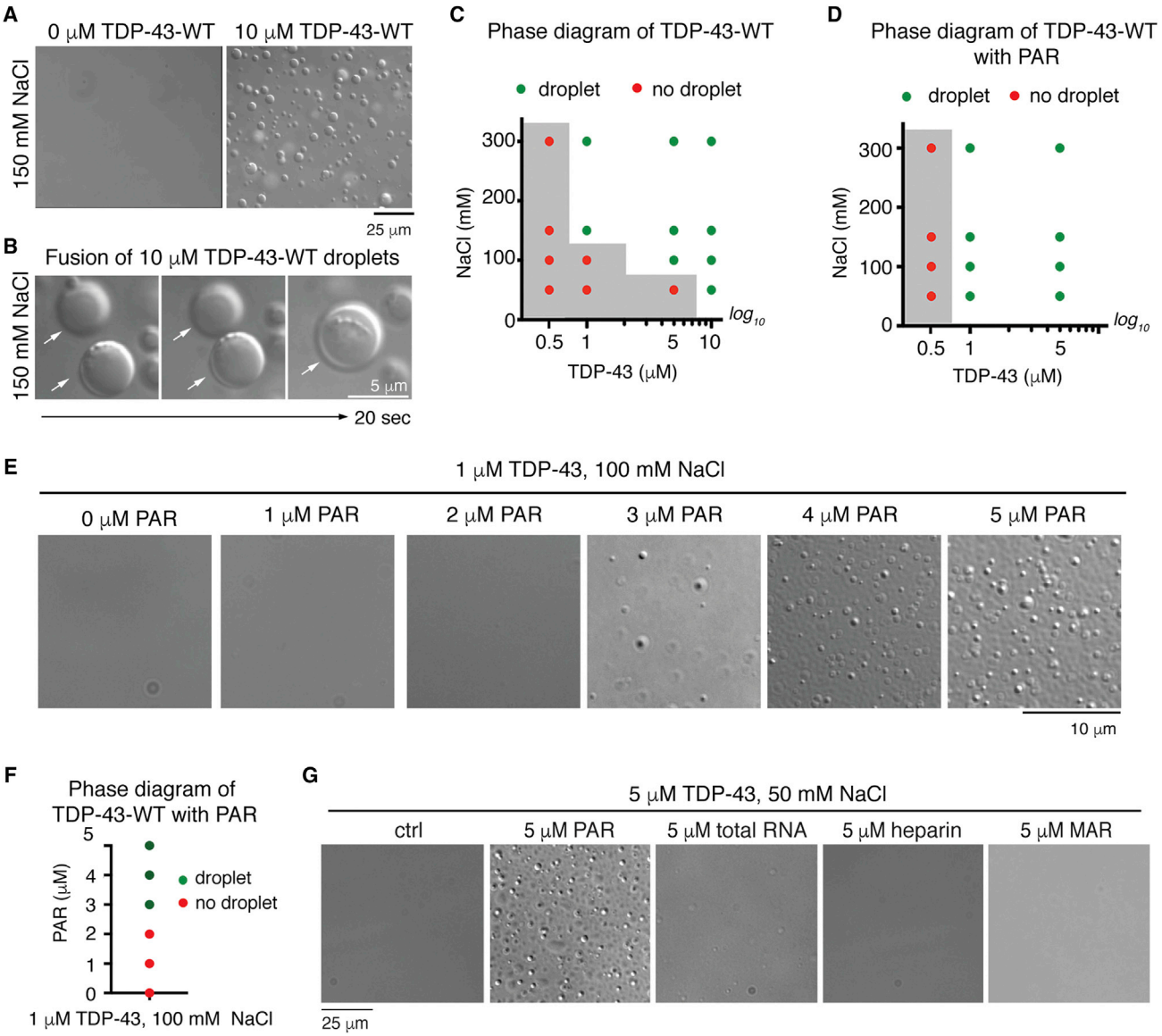

Figure 3. PAR Promotes LLPS of TDP-43 *In Vitro*

(A) Spontaneous LLPS of 10 μM SUMO-TDP-43-WT in 150 mM NaCl. The experiment was repeated more than five times on two preparations of protein.

(B) Fusion of two TDP-43-WT droplets (white arrows).

(C) The presence (green) or absence (red) of TDP-43-WT droplets. The gray area indicates the phase boundary. The results were confirmed in two independent protein preparations. Conditions on either side of the phase boundary were repeated three times.

(D) PAR reduced the phase boundary of TDP-43 LLPS. The presence (green) or absence (red) of protein droplets is plotted, and the gray area indicates the phase boundary. The results were confirmed in two independent protein preparations. Conditions at the phase boundary (gray side) were repeated three times.

(E) Addition of PAR (1–5 μM mono(ADP-ribose) equivalents) promoted TDP-43-WT LLPS in a dose-dependent manner. This was performed on one protein preparation.

(F) The presence (green) or absence (red) of TDP-43 droplets.

(G) PAR promoted 5 μM TDP-43-WT LLPS in 50 mM NaCl. Heparin, yeast total RNA, and mono(ADP-ribose) (MAR) at the same concentration had no effect. The experiment was repeated twice from 1 protein preparation.

All experiments were performed at room temperature. See also Figure S2.

PAR could regulate this process. We used conditions that mimic the intracellular environment. We included dextran as a macromolecular crowding agent and buffer conditions of physiological salt (150 mM NaCl and pH 7.5), and we employed physiological (Ling et al., 2010) TDP-43 concentrations (1–10 μM). Under these conditions, purified TDP-43 (His_6-small ubiquitin-like modifier [SUMO]-TDP-43-WT) (Figure S2B) spontaneously formed dynamic spherical droplets that fused and increased in size, indicating liquid-like properties (Figures 3A and 3B; Video S1). LLPS of TDP-43 was induced at lower TDP-43 concentrations

by increasing the salt (NaCl) concentration (Figure 3C). Thus, LLPS of full-length TDP-43 can be achieved under physiological conditions and is dependent on TDP-43 and salt concentrations.

To evaluate whether PAR could promote LLPS of TDP-43, we lowered the concentration of TDP-43 to 1 μM and the salt concentration to 100 mM; under these conditions, TDP-43 did not undergo LLPS (Figure 3C). The addition of PAR (1–5 μM ADP-ribose equivalents) at a chain length ranging from 2–300 ADP-ribose subunits stimulated TDP-43 LLPS in a dose-dependent manner (Figures 3D–3F). At lower protein and salt concentrations, 5 μM PAR promoted LLPS of TDP-43 (Figure 3D and S2E) and lowered the phase boundary. By contrast, addition of heparin, total RNA, mono(ADP-ribose), or BSA did not stimulate TDP-43 LLPS, and PAR did not undergo LLPS in the absence of protein (Figures 3G and S2F–S2J). Finally, we purified TDP-43 as a C-terminally tagged MBP fusion protein (TDP-43-WT-MBP-His_6) (Figure S2C). Under physiological salt conditions (150 mM NaCl) and with dextran, TDP-43-WT-MBP spontaneously formed liquid droplets (Figure S2K), and the addition of PAR to TDP-43-WT-MBP promoted LLPS (Figure S2L). Thus, PAR-mediated LLPS of TDP-43 is a feature of TDP-43 and is independent of the protein tag.

We next asked whether PAR-regulated LLPS of TDP-43 required the PAR-binding motifs in the NLS (Figure 2). Under conditions in which TDP-43 phase-separated, TDP-43 with mutation in both PAR-binding motifs (His_6-SUMO-TDP-43-ΔPBM) (Figure S2B) formed irregular structures that were smaller in size and did not fuse, indicating an aberrant phase transition to solid-like states (Figures 4B and 4C). At a lower salt concentration (50 mM NaCl), TDP-43-ΔPBM remained diffuse, indicating that transition into a solid state is salt-dependent (Figure 4C). In support of our conclusion that the NLS harbors functional PAR-binding motifs, the addition of PAR failed to promote LLPS of TDP-43-ΔPBM (Figures 4D and 4E; Figure S2M). Thus, the PAR-binding motifs are critical for normal LLPS of TDP-43.

Disease-Associated TDP-43 Has Altered LLPS Dynamics

In disease, TDP-43 can become N-terminally truncated (Igaz et al., 2009; Neumann et al., 2006, 2009), raising the possibility that fragments of TDP-43 that accumulate in disease may have impaired LLPS properties. To assess this, we examined a 35-kDa isoform of TDP-43 identified in ALS spinal cord tissue (Xiao et al., 2015) and a 25-kDa fragment of TDP-43 identified in ALS brain tissue (Kametani et al., 2016). The fragments were purified as His_6-SUMO-tagged fusion proteins (His_6-SUMO-TDP-43-C35 and His_6-SUMO-TDP-43-C25) (Figures 4A and S2B). Under conditions where TDP-43-WT phase-separated, TDP-43-C35, which retains PBM2, formed small, spherical structures that did not fuse, whereas the C25 fragment formed filamentous aggregates (Figures 4B and 4C), indicating that they both lacked liquid properties. Moreover, PAR was ineffective at promoting LLPS of TDP-43-C35 or TDP-43-C25 at all salt and protein concentrations tested (Figures 4D and 4E; Figure S2M). Collectively, these advances highlight that the N-terminal region and the PBMs are critical for TDP-43 liquid demixing.

To assess the effect of an ALS-linked mutation on PAR-stimulated LLPS of TDP-43, we expressed and purified TDP-43 with an ALS-linked mutation, Q331K (His_6-SUMO-TDP-43-Q331K) (Figure S2D), previously shown to promote aggregation (Johnson et al., 2009). Surprisingly, the Q331K mutation did not completely prevent TDP-43 from forming protein droplets (Figures 4B and 4C); however, the droplets were fewer in number, and, at lower NaCl concentrations, the droplets coexisted with irregular solid structures (Figures 4B and 4C and S2M and S2N). At low NaCl concentrations, PAR promoted the aggregation of solid irregular structures of TDP-43-Q331K (Figures 4D and 4E) and was ineffective at higher salt concentrations (Figure S2M). Together, these data suggest that the Q331K mutation is defective in LLPS and that the propensity to aggregate can be stimulated by PAR.

The PBMs Are Required for TDP-43 Stress Granule Localization

We extended these findings to the intracellular milieu of mammalian cells. Under normal conditions, PAR levels are low, and TDP-43 is predominantly nuclear; however, upon stress, PAR and TDP-43 form foci in the cytoplasm (Figures S3A–S3C). PAR is a constituent of mammalian stress granules (Catara et al., 2017; Leung et al., 2011); hence, we co-labeled the cells with the stress granule markers eIF3, T-cell-restricted intracellular antigen 1 (TIA-1)-related protein (TIAR), Ataxin-2, and PAR (Figures S3B–S3E) to reveal that TDP-43 and PAR coexist in stress granules (Figures 2A–S2C). To ascertain whether the PBMs in the NLS regulated TDP-43 localization to PAR-containing stress granules, we expressed TDP-43-YFP and immunostained for PAR. This revealed that mutation of the PBM reduced PAR labeling of TDP-43-YFP from 93% ± 2% to 17.6% ± 4.9% (SEM) (Figures S3F–S3H). These data indicate that mutation in the PBM reduces the ability of TDP-43 to interact with PAR in mammalian cells, and are in support of our data that the PBMs mediate binding to PAR (Figure 2).

To determine whether mutation in the PBM also reduced TDP-43 localization to stress granules, we rigorously characterized TDP-43-GFP before and after stress. As anticipated, TDP-43-WT-GFP was predominantly nuclear (Figure 5B), whereas mutation in the PBMs (TDP-43-ΔPBM-GFP), which is known to prevent nuclear localization (Winton et al., 2008), resulted in diffuse cytoplasmic accumulation (Figure 5B). Upon stress, the percentage of cells with cytoplasmic foci of TDP-43-WT and TDP-43-ΔPBM increased to 23.7% ± 3% and 89.7% ± 4.9% (SEM), respectively (Figures 5A–5C and S3I and S3J); furthermore, the stress-induced foci of TDP-43-WT, but not TDP-43-ΔPBM, co-labeled with the stress granule markers G3BP1 and TIAR (Figures 5B, 5D–5F, and S3I–S3K). Staining with additional markers of stress granules (Ataxin-2 and eIF3) in mammalian cells, immunostaining with TIAR in rat primary neurons, and exposure to a different stress (heat shock) confirmed that TDP-43-WT was recruited to PAR-containing stress granules, whereas stress-induced foci of TDP-43-ΔPBM were excluded from these stress granules (Figures S4A–S4F). Together, these data suggest that a functional PBM is required for TDP-43 to localize to stress granules.

To determine whether PAR binding was necessary for TDP-43 recruitment to stress granules, we added an exogenous PBM from hnRNPA2/B1 (Gagné et al., 2003) to TDP-43-ΔPBM (Figure 5A). The PBM in hnRNPA2/B1 is distinct from the NLS and

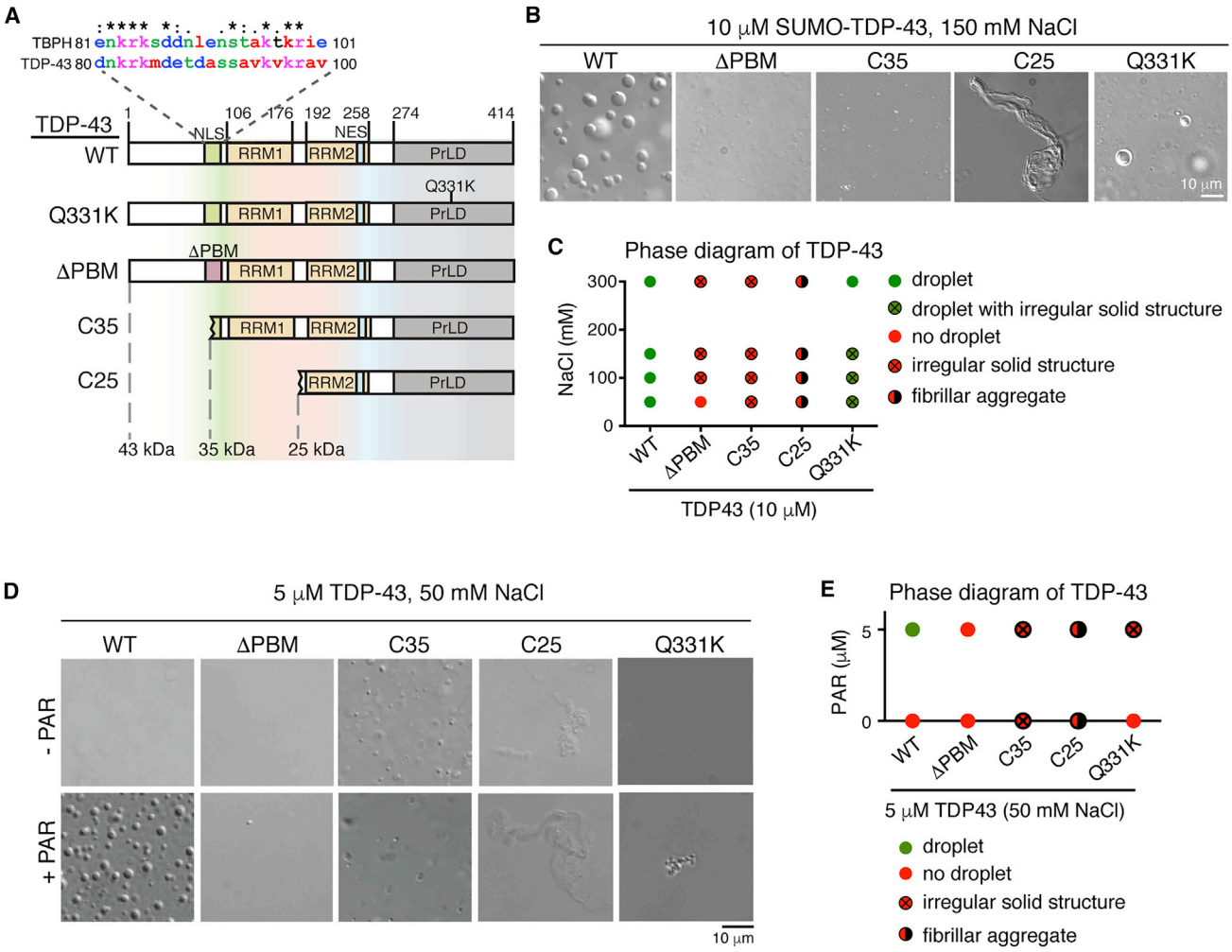

Figure 4. The PAR-Binding Region and the N Terminus Are Required for TDP-43 LLPS *In Vitro*

(A) The NLS of human TDP-43 and the *Drosophila* homolog TAR DNA-binding protein-43 homolog (TBPH) share 42.9% identity. The protein domains of TDP-43-WT, TDP-43-Q331K, TDP-43-ΔPBM, TDP-43-C35 (amino acids 85–414), and TDP-43-C25 (amino acids 176–414) are shown.

(B) LLPS of 10 μM protein in 150 mM NaCl. SUMO-TDP-43-WT underwent LLPS, but SUMO-TDP-43-ΔPBM and SUMO-TDP-43-C35 formed irregular solid structures that did not fuse. SUMO-TDP-43-C25 formed fibrillar aggregates. TDP-43-Q331K formed liquid droplets and the occasional irregular solid structure. The experiment was performed three independent times with two protein preparations of TDP-43-WT, C35, and C25 and twice with one protein preparation of TDP-43-Q331K.

(C) The presence of liquid droplets, no liquid droplets, irregular solid structures, both liquid droplets and irregular solid structures, and fibrillar aggregates is plotted.

(D) LLPS at 5 μM protein and 50 mM NaCl. PAR at 5 μM equivalents to ADP-ribose promoted LLPS of TDP-43-WT and did not promote LLPS of TDP-43-ΔPBM, TDP-43-C35, and TDP-43-C25. PAR promoted the formation of irregular solid structures of TDP-43-Q331K. The experiment was performed three independent times with two independent protein preparations.

(E) The presence of liquid droplets, no liquid droplets, irregular solid structures, and fibrillar aggregates is plotted for each TDP-43 variant in the absence and presence of PAR.

All experiments were performed at room temperature. See also Figure S2.

is situated in the N-terminal domain between the two RNA recognition motifs (RRMs) (Gagné et al., 2003). Under normal conditions, TDP-43-ΔPBM$_{PBM\text{-}A2/B1}$ was diffusely enriched in the cytoplasm (Figure 5B), indicating that the PBM of hnRNPA2/B1 did not alter the cellular distribution of TDP-43-ΔPBM. The application of stress initiated the formation of cytoplasmic TDP-43-ΔPBM-$_{PBM\text{-}A2/B1}$ foci (Figures 5B and 5C). Strikingly, the exogenous PBM significantly increased the percentage of cells with TDP-43-ΔPBM localized to G3BP1-labeled stress granules from 0.6% ± 0.4% (SEM) to 23.7% ± 9% (Figures 5D–5F). Thus, the addition of a functional PAR-binding motif is sufficient to restore stress-granule accumulation of TDP-43 defective in PAR binding (TDP-43-ΔPBM). We suggest that the localization of TDP-43 to stress granules is dependent on PAR-binding.

We next addressed whether the C-terminal fragments of TDP-43, which lack the N terminus and PBMs, could localize

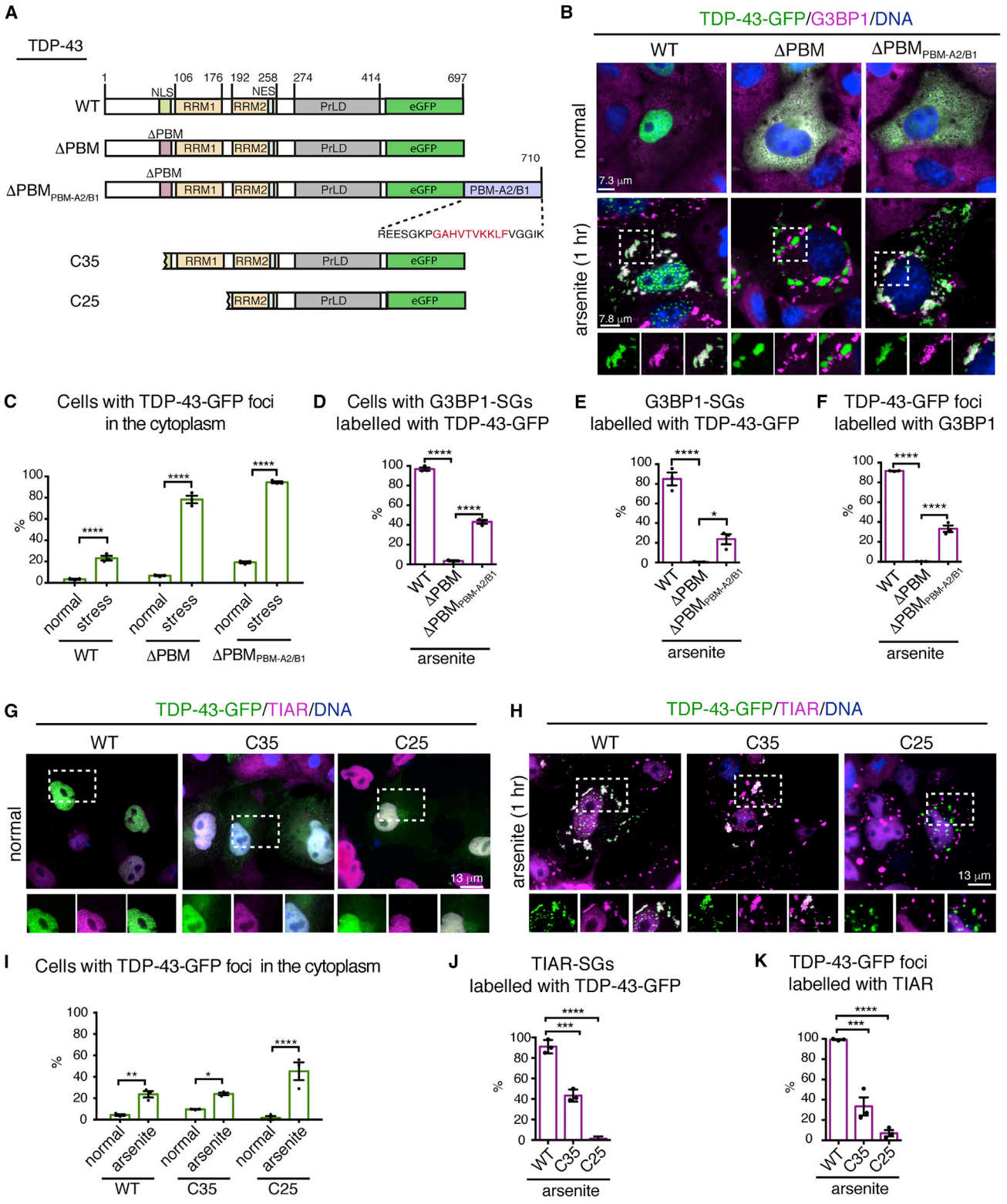

Figure 5. The PAR-Binding Region Is Required for the Recruitment of TDP-43 to Stress Granules

(A) Domain architecture of TDP-43-WT, TDP-43-ΔPBM, TDP-43-$\Delta PBM_{PBM-A2/B1}$, TDP-43-C35, and TDP-43-C25. The peptide sequence added to the C terminus of TDP-43-$\Delta PBM_{PBM-A2/B1}$ is indicated. Red amino acids show the PBM of hnRNPA2/B1, with flanking amino acids of hnRNAPA2/B1 shown in black.

(legend continued on next page)

to stress granules. TDP-43-C35-GFP and TDP-43-C25-GFP, which normally diffusely localized to the nucleus and cytoplasm, formed cytoplasmic foci upon arsenite treatment (Figures 5F–5I). TDP-43-C35 retains PBM2 and localized to 43.5% ± 3.4% (SEM) of TIAR-labeled stress granules (Figures 5F–5H). By contrast, TDP-43-C25 localized to 2.3% ± 1.3% (SEM) of TIAR-labeled stress granules (Figures 5F–5H). These data indicate that the N-terminal region of TDP-43 is important for the recruitment of the protein to stress granules and suggest that, in disease, stress-granule recruitment of the C-terminal fragments of TDP-43 will be partially (C35) or almost fully (C25) impaired.

Recruitment to Stress Granules Inhibits Phosphorylation of TDP-43

A long-standing notion is that TDP-43 recruited to stress granules becomes marked with the phosphorylation hallmark of disease (Li et al., 2013). To test this, we examined phosphorylation of TDP-43 foci that were localized to, or excluded from, stress granules. Surprisingly, staining for the disease-specific phosphorylation mark pS409/10 revealed that arsenite-induced and heat-induced foci that were excluded from stress granules (TDP-43-ΔPBM, C35, and C25), but not TDP-43 localized to stress granules (TDP-43-WT), were phosphorylated (Figures 6A–6C and S5A–S5E). We then examined the phosphorylation status of TDP-43-ΔPBM with an exogenous PBM (TDP-43-$\Delta PBM_{PBM\text{-}A2/B1}$). Importantly, the percentage of cells with arsenite-induced cytoplasmic foci of TDP-43-$\Delta PBM_{PBM\text{-}A2/B1}$ that co-labeled with pS409/10 was indistinguishable from TDP-43-WT (Figures S6D–S6F), indicating that the exogenous PBM was sufficient to both localize TDP-43-ΔPBM to stress granules (Figure 5) and prevent stress-induced phosphorylation.

Next we established a live-cell assay to examine the internal dynamics of stress-induced foci of TDP-43. Diffuse TDP-43-WT and TDP-43-ΔPBM in the cytoplasm recovered rapidly from photobleaching (Figures S5F and S5G), indicating that the two proteins were normally highly mobile. By contrast, stress-induced, cytoplasmic foci formed by both proteins were immobile (Figures S5F and S5G). However, the stress-induced foci of TDP-43-WT resolved after the removal of stress, whereas the forms of the protein that aggregated outside of the stress granule persisted (Figure S5H). These data indicate that localization of TDP-43 to the stress granule environment is critical for preventing stress-induced phosphorylation and for the resolution of TDP-43 foci upon recovery from stress.

We next determined whether there were conditions of stress that could promote phosphorylation of TDP-43-WT. Intriguingly, low levels of prolonged stress (25 μM arsenite for 6 hr) led to an increase in the percentage of cells with cytoplasmic TDP-43-WT foci, the majority (81% ± 6% [SEM]) of which were phosphorylated and devoid of the stress granule protein eIF3 (Figures S6A–S6E). In addition, exposure to high levels of stress for a prolonged period (0.5 mM arsenite for 4 hr) led to the formation of, and the subsequent resolution of, G3BP1-labeleld stress granules (Figure 7A). By contrast, stress-induced foci of TDP-43-WT were sustained over this time period (Figure 7B), and in 78% ± 8% (SEM) of cells, the TDP-43-WT foci were immunolabeled for pS409/10 and devoid of G3BP1 (Figures 7C and 7D). Thus, consistent with our finding that the stress granule environment inhibits S409/410 phosphorylation, prolonged stress induces the formation of phosphorylated TDP-43-WT foci in the absence of stress granules.

Small-Molecule Inhibition of Tankyrase Inhibits Stress-Induced Foci of TDP-43

Our studies were launched by the discovery that lowered levels of *tankyrase* mitigate TDP-43-elicited neurodegeneration in the fly. We thus examined the role of Tankyrase to modulate stress-induced foci of TDP-43 in mammalian cells. In mammals, there are two Tankyrase homologs, Tankyrase 1 and Tankyrase 2 (also known as PARP-5a and PARP-5b), which share 82% sequence similarity and are collectively detected as Tankyrase 1/2 (Citarelli et al., 2010). Under stress, Tankyrase-1/2 localized to 35% ± 9% (SEM) of Ataxin-2-labeled stress granules and to 31% ± 2% (SEM) of TIAR-labeled stress granules (Figure S7A). Thus, Tankyrase 1/2 is not a constitutive stress granule protein.

Tankyrase-1/2 inhibitors have been developed as anti-proliferative agents for cancer cells (Mariotti et al., 2017). We examined small-molecule inhibition of Tankyrase-1/2 for an effect on stress granule biogenesis and TDP-43 focus assembly. Treatment with

(B) Normally, TDP-43-WT was nuclear, and TDP-43-ΔPBM and TDP-43-$\Delta PBM_{PBM\text{-}A2/B1}$ were cytoplasmic. Upon arsenite treatment, TDP-43-WT and TDP-$PBM_{PBM\text{-}A2/B1}$ localized to stress granules whereas TDP-43-ΔPBM was excluded from stress granules. Cells were exposed to 0.5 mM sodium arsenite for 1 hr, labeled for G3BP1, and stained with Hoechst.

(C) The percentage of cells with cytoplasmic TDP-43-GFP foci. Mean (± SEM), n = 3, two-way ANOVA ($p < 0.0001$), and Holm-Sidak's test. Asterisks, significant.

(D) The percentage of cells with one or more G3BP1-labeled stress granule (SG) co-labeled with TDP-43-GFP. Mean (± SEM), n = 3, one-way ANOVA ($p < 0.0001$), and Tukey's test. Asterisks, significant.

(E) The percentage of G3BP1-labeled SGs co-labeled with TDP-43-GFP. Mean (± SEM), n = 3, one-way ANOVA ($p < 0.0001$), and Tukey's test. Asterisks, significant.

(F) The percentage of TDP-43-GFP foci co-labeled with G3BP1. Mean (± SEM), n = 3, one-way ANOVA ($p < 0.0001$), and Tukey's test. Asterisks, significant.

(G) Under normal conditions TDP-43-WT-GFP was diffusely nuclear, whereas TDP-43-C35-GFP and TDP-43-C25-GFP were diffusely nuclear and cytoplasmic. Cells were labelled for TIAR and stained with Hoescht (DNA).

(H) Foci of TDP-43-C35 and TDP-43-C25-GFP are largely excluded from stress granules. Cells were exposed to 0.5 mM sodium arsenite for 1 hr, labeled for TIAR, and stained with Hoechst (DNA).

(I) The percentage of cells with cytoplasmic TFP-43-GFP foci. Mean (± SEM), n = 3, two-way ANOVA ($p = 0.0042$), and Holm-Sidak's test. Asterisks, significant.

(J) The percentage of TIAR-labeled stress granules (SGs) co-labeled with TDP-43-GFP. Mean (± SEM), n = 3, two-way ANOVA ($p < 0.0001$), and Tukey's test. Asterisks, significant.

(K) The percentage of TDP-43-GFP foci co-labeled with TIAR. Mean (± SEM), n = 3, one-way ANOVA ($p < 0.0001$), and Tukey's test. Asterisks, significant. *$p < 0.05$, **$p < 0.01$, ***$p < 0.001$, and ****$p < 0.0001$.

See also Figures S3 and S4.

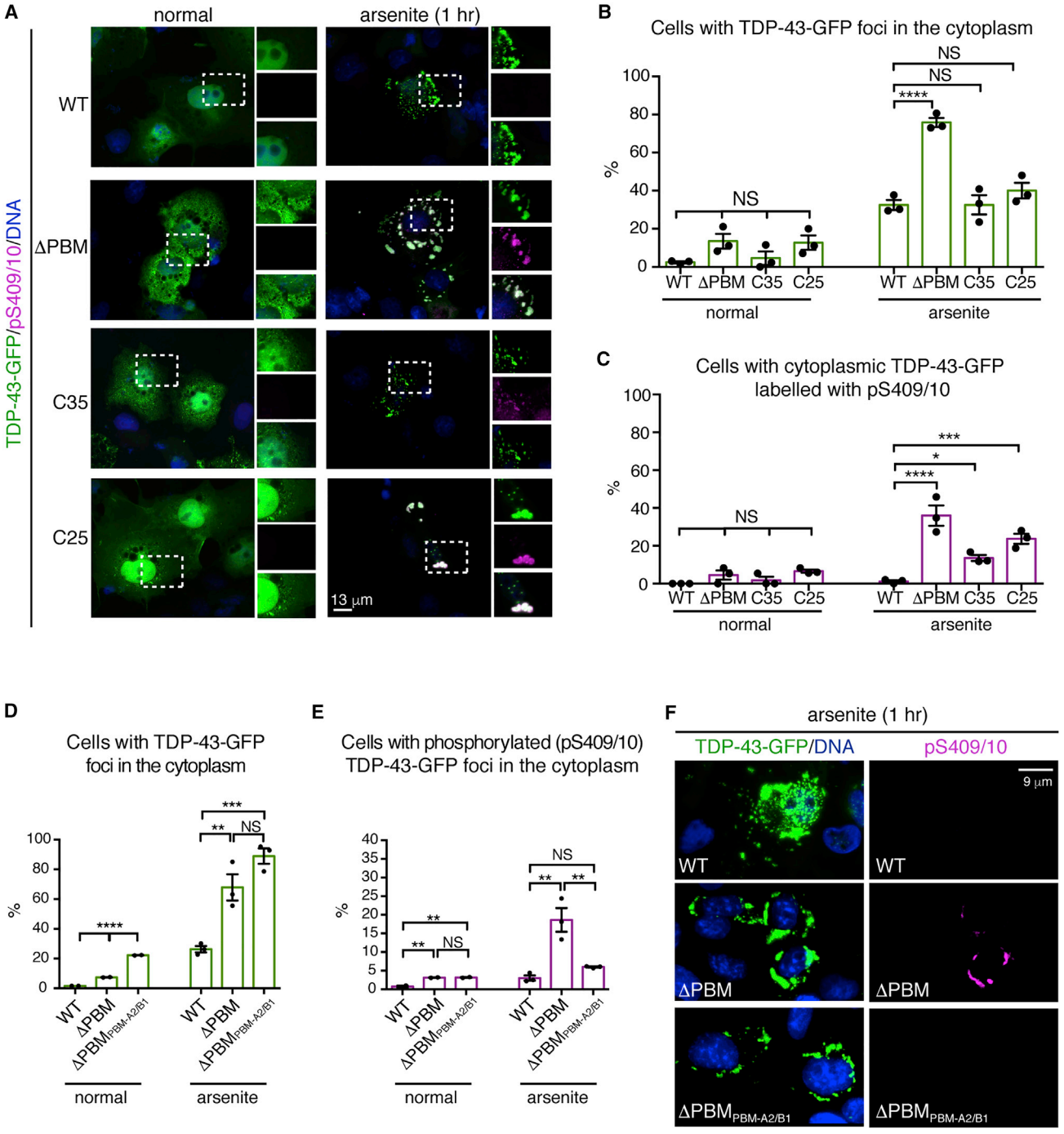

Figure 6. Initial Recruitment to Stress Granules Protects TDP-43 from Phosphorylation

(A) Stress induced the formation of phosphorylated (pS409/10) foci of TDP-43-ΔPBM, TDP-43-C35, and TDP-43-C25 but not TDP-43-WT. Cells were stressed with 0.5 mM arsenite for 1 hr and labeled for pS409/10 and Hoechst (DNA).

(B) The percentage of cells with cytoplasmic TDP-43-GFP foci. Mean (± SEM), n = 3, two-way ANOVA ($p < 0.0001$), and Tukey's test. Asterisks, significant.

(C) The percentage of cells with cytoplasmic TDP-43 foci co-labeled with pS409/10. Mean (± SEM), n = 3, one-way ANOVA ($p < 0.0001$), and Tukey's test. Asterisks, significant.

(D) The percentage of cells with cytoplasmic TDP-43-GFP (WT, ΔPBM, or $\Delta PBM_{PBM\text{-}A2/B1}$) foci. Mean (± SEM), n = 3, one-way ANOVA, and Dunnett's test ($p < 0.001$). Asterisks, significant.

(legend continued on next page)

the inhibitor XAV939 (Huang et al., 2009) markedly reduced the formation of arsenite-induced cytoplasmic foci of TDP-43-WT-GFP without altering the percentage of cells with G3BP1-labeled stress granules (Figures 7E–7G). Two additional inhibitors, G007-LK and IWR-1-endo, with little to no effect on PARP-1/2 activity (Huang et al., 2009; Voronkov et al., 2013) behaved similarly (Figures 7E and 7G and S7E–S7G). Thus, Tankyrase-1/2 activity regulates the formation of cytoplasmic TDP-43 foci but not stress granule formation. Together, our data suggest that reduced Tankyrase-1/2 activity mitigates ALS-associated degeneration by reducing the cytoplasmic localization of TDP-43 and subsequent neurodegeneration.

DISCUSSION

Our data has led to a two-step model for regulation of TDP-43 whereby Tankyrase-1/2 regulates the formation of cytoplasmic foci of TDP-43 and PAR regulates the recruitment of TDP-43 to stress granules. Under prolonged stress, stress-induced foci of TDP-43 become marked with the disease signature of phosphorylation. Importantly, small-molecule inhibitors of Tankyrase reduce the formation of TDP-43 foci in the cytoplasm. Thus, Tankyrase regulates the subcellular localization of TDP-43 and mitigates TDP-43-mediated neurodegeneration. Small-molecule inhibitors of Tankyrase-1/2 may provide a therapeutic strategy for ALS/FTD.

The N-Terminal Domain and PBMs Regulate TDP-43 LLPS and Stress Granule Recruitment

We have defined functional PBMs embedded in the TDP-43 NLS that are required for TDP-43 LLPS. Mounting evidence implicates the N-terminal domain of TDP-43 as critical for higher-order assemblies (Afroz et al., 2017; Chang et al., 2012; Jiang et al., 2017; Mompeán et al., 2016; Romano et al., 2015; Zhang et al., 2013). Our data, and a report that that pinpoints serine 48 in the N-terminal domain (Wang et al., 2018), indicate that the N-terminal domain is also critical for TDP-43 phase separation *in vitro*. We show that the negatively charged PAR biopolymer can initiate LLPS of TDP-43 and suggest that this occurs via multivalent interactions with the PBM in the N-terminal domain.

In the cellular milieu, TDP-43 is not a ubiquitous stress granule protein and does not readily localize to the cytoplasm (Bentmann et al., 2012; Cohen et al., 2012; Dewey et al., 2011). Previous studies have focused on TDP-43 with mutation in the NLS without a comparison with the WT protein (Bentmann et al., 2012; Nonaka et al., 2009). Here, by successfully inducing the accumulation of TDP-43-WT in the cytoplasm, we were able to uncover the essential role of the PAR binding and N-terminal regions for the recruitment of TDP-43 to stress granules. Importantly, the addition of the PAR-binding motif from hnRNPA2/B1 to TDP-43-ΔPBM was sufficient to re-localize TDP-43-ΔPBM back to stress granules. The PBM from hnRNPA1/B2 did not alter the cytoplasmic localization of TDP-43-ΔPBM, suggesting that the lack of stress granule recruitment was not a result of a loss of nuclear localization but due to loss of PAR binding. Direct PARylation of specific stress granule proteins assists with stress granule formation (Leung et al., 2011), and we propose that non-covalent PAR-binding is an added means by which proteins enter stress granules. Interestingly, the C35 fragment retains PBM2 and is only partially localized to stress granules upon stress. The partial exclusion of C35 and the almost complete exclusion of C25 from stress granules could be due to a lack of binding to the PAR scaffold or because these forms of TDP-43 undergo aberrant phase separation.

Recruitment to Stress Granules Inhibits Phosphorylation of TDP-43

Our studies refine the long-standing model that stress granule localization of TDP-43 nucleates disease-associated pathology (Li et al., 2013). We present a model whereby TDP-43 foci excluded from stress granules readily transition into disease-like aggregates. Various kinases promote stress granule biogenesis (Kedersha et al., 2013), and it is possible that TDP-43 aggregates excluded from stress granules are exposed to and phosphorylated by these stress-responsive kinases. We suggest that an additional role of stress granules is to protect proteins from the activated kinases during cellular stress. In disease, the phosphorylation and aggregation of C35 and C25 may arise from a failure to phase-separate and localize to stress granules. TDP-43 that can localize to stress granules becomes phosphorylated upon long-term stress and in the absence of stress granules. This finding may explain why only a subset of TDP-43 inclusions in the post-mortem spinal cord co-labels with stress granule components (Bentmann et al., 2012; Colombrita et al., 2009; McGurk et al., 2014). Stress granule protein may become trapped in TDP-43 aggregates as the stress granules dissolves. Thus, in the spinal cord, TDP-43 may be recruited to stress granules and be protected but may transition to a pathological aggregated state as a result of the stress granule dissolution process.

Tankyrase-1/2 as a Potential Therapeutic Strategy in ALS and FTD

It has been reported that upregulation of Tankyrase-1 promotes stress granule formation (Leung et al., 2011). Our studies uncover that Tankyrase-1/2 is not a ubiquitous stress granule protein and that Tankyrase-1/2 inhibition does not alter the formation of G3BP1-labeled stress granules. It is possible that Tankyrase-mediated regulation of stress granules may be independent of enzymatic activity or may only occur in select stress granules or on select proteins such as TDP-43. We hypothesize that Tankyrase-1/2 acts upstream of TDP-43 recruitment to stress granules and may regulate the transport of TDP-43 to stress granules. Although stress granule localization is initially protective, prolonged stress leads to phosphorylated

(E) The percentage of cells with cytoplasmic TDP-43-GFP (WT, ΔPBM, or $\Delta PBM_{PBM\text{-}A2/B1}$) foci co-labeled with pS409/10. Mean (± SEM), n = 3, one-way ANOVA, and Dunnett's test (normal, $p < 0.0001$; arsenite, $p = 0.0024$).

(F) Stress induced the phosphorylation of cytoplasmic foci of TDP-43-ΔPBM-GFP foci but not TDP-43-WT-GFP or TDP-43-$\Delta PBM_{PBM\text{-}A2/B1}$-GFP. Cells exposed to 0.5 mM arsenite (1 hr) were labeled for pS409/10 and Hoechst.

See also Figures S5 and S6.

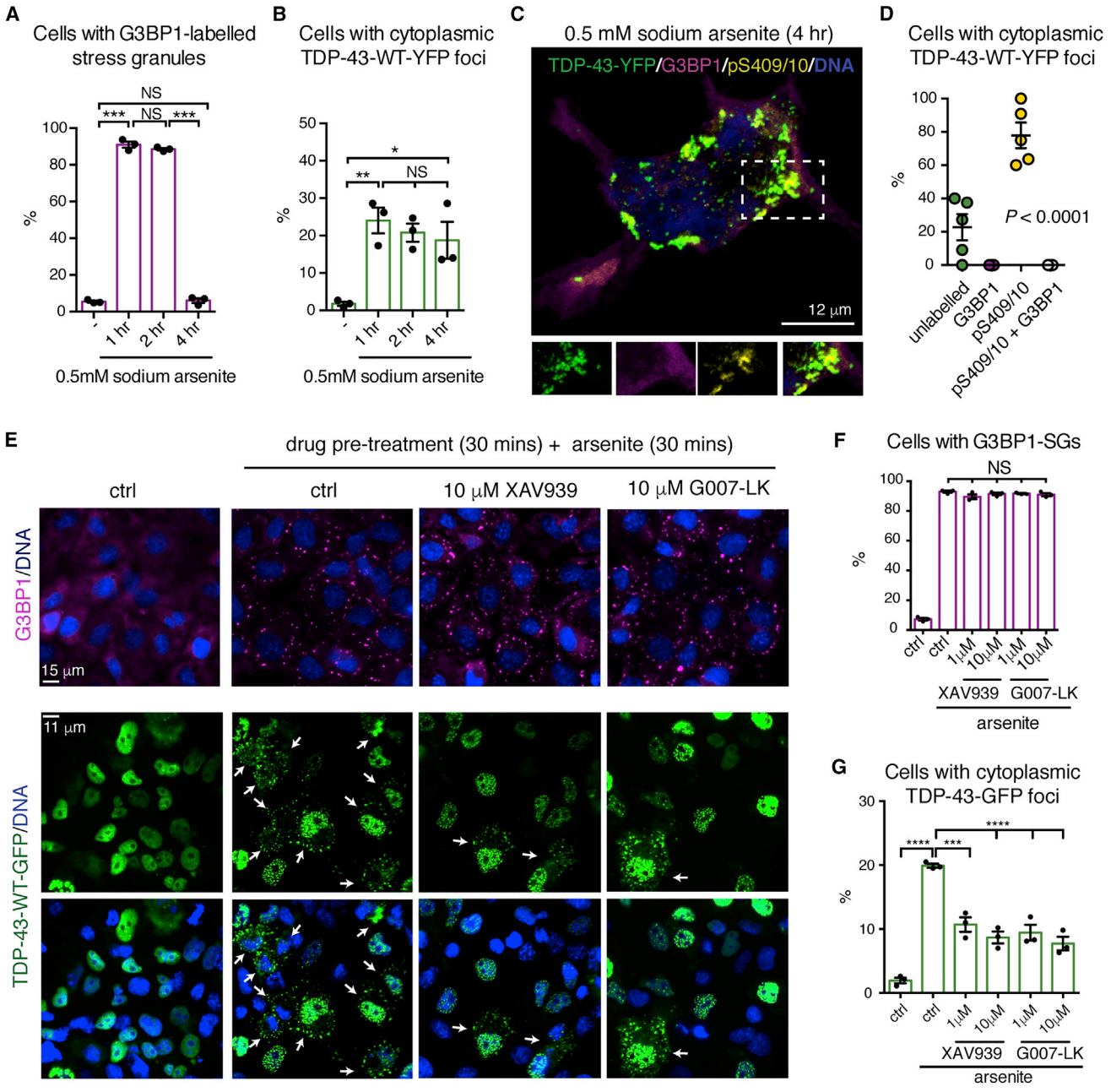

Figure 7. Prolonged Stress Leads to the Phosphorylation of TDP-43 Foci, and TDP-43 Focus Formation Can Be Mitigated with Small-Molecule Inhibitors of Tankyrase-1/2

(A) G3BP1-labeled stress granules resolved after 4 hr exposure to 0.5 mM arsenite. Mean (± SEM), n = 3, one-way ANOVA ($p = 0.005$), and Tukey's test. Asterisks, significant.

(B) Stress-induced foci of TDP-43-WT-YFP persisted after 4 hr exposure to 0.5 mM arsenite. Mean (± SEM), n = 3, one-way ANOVA ($p < 0.0001$), and Tukey's test. Asterisks, significant.

(C) Cytoplasmic TDP-43-WT-YFP foci formed in 0.5 mM arsenite (4 hr) were co-labeled for pS409/10 but not G3BP1. Cells were labeled for G3BP1, pS409/10, and Hoechst and imaged by confocal microscopy.

(D) Confocal images of cells with cytoplasmic TDP-43-WT-YFP foci were quantified. Mean (± SEM), n = 5, one-way ANOVA ($p < 0.0001$).

(E) Cells left untreated or treated with 0.5 mM arsenite (30 min) in the absence or presence of XAV939 or G007-LK. A 30-min pretreatment was required, and lack of a dose response is likely due to being above the concentration of inhibitor where the response is reduced by 50% (IC_{50}) (Figures S7H and S7I). Arrows, cells with cytoplasmic TDP-43-WT-GFP foci. Cells were labeled for G3BP1 and Hoechst.

(legend continued on next page)

aggregates. A potential therapeutic strategy could be to target Tankyrase-1/2 activity to inhibit the initial accumulation of TDP-43 in the cytoplasm. Our studies bring PARylation in ALS/FTD to the forefront and specifically implicate Tankyrase inhibitors as potential therapeutics in ALS/FTD.

STAR★METHODS

Detailed methods are provided in the online version of this paper and include the following:

- KEY RESOURCES TABLE
- CONTACT FOR REAGENT AND RESOURCE SHARING
- EXPERIMENTAL MODEL AND SUBJECT DETAILS
  - *Drosophila* stocks and maintenance
  - Mammalian cells and culture details
  - Rat cortical neuron cultures
- METHOD DETAILS
  - *Drosophila* external eye imaging and histology
  - *Drosophila* lifespan
  - Nuclear Cytoplasmic fractionation
  - Immunoblotting of *Drosophila* total protein
  - Real-time PCR
  - Co-immunoprecipitation
  - Plasmids
  - Cell stress assays and immunofluorescence
  - Image quantification and statistics
  - Fluorescence recovery after photobleaching
  - GST-TDP-43 protein purification
  - PAR polymer
  - PAR-binding dot blot assay
  - Purification of Recombinant His_6-SUMO-TDP-43
  - Purification of Recombinant TDP-43-MBP-His_6
  - Liquid-droplet formation
- QUANTIFICATION AND STATISTICAL ANALYSIS
- DATA AND SOFTWARE AVAILIBILITY

SUPPLEMENTAL INFORMATION

Supplemental Information includes seven figures and one video and can be found with this article online at https://doi.org/10.1016/j.molcel.2018.07.002.

ACKNOWLEDGMENTS

We thank Yanlan Huang, Jeffrey Nirschl, and Yongqing Zhu for technical assistance. We thank Lindsey D. Goodman for reading the manuscript and for insightful comments, the CDB Microscopy Core at the University of Pennsylvania for the use of their Leica TCS SP8 confocal microscope, and Nicolas L. Fawzi (Brown University, USA) for the TDP-43-MBP-His_6 plasmid DNA. This work was funded by grants from the Ellison Medical Foundation (to L.G.), the American Federation for Aging Research (to L.G.), the Alzheimer's Association (to L.G.), the Life Extension Foundation (to J.S.), the ALS Association (to J.S.), a Department of Biochemistry and Biophysics pilot grant (to J.S.), Target ALS (to J.S. and N.M.B.), the Glenn Foundation (to N.M.B.), the Robert Packard Center for ALS Research at Johns Hopkins (to J.S.), and NIH R01 NS095746-01 (to R.G.K.), R21NS093439 (to R.G.K.), 5R21NS087077-02 (to R.G.K.), R01GM099836 (to J.S.), R21NS090205 (to J.S.), 5R01NS073660 (to N.M.B.), and R35NS097275 (to N.M.B.).

AUTHOR CONTRIBUTIONS

L.M. conceived, designed, and performed experiments, performed statistical analysis, and analyzed data. E.G. designed and performed experiments and analyzed data. V.T. performed experiments. J.M.-P., L.G., and R.G.K. contributed reagents and materials. R.G.K., J.S., and N.M.B. conceived and designed experiments, analyzed data, and supervised the research. L.M., J.S., and N.M.B. wrote the manuscript.

DECLARATION OF INTERESTS

The authors declare no competing interests.

Received: January 24, 2018
Revised: May 18, 2018
Accepted: June 29, 2018
Published: August 9, 2018

REFERENCES

Afroz, T., Hock, E.M., Ernst, P., Foglieni, C., Jambeau, M., Gilhespy, L.A.B., Laferriere, F., Maniecka, Z., Plückthun, A., Mittl, P., et al. (2017). Functional and dynamic polymerization of the ALS-linked protein TDP-43 antagonizes its pathologic aggregation. Nat. Commun. *8*, 45.

Becker, L.A., Huang, B., Bieri, G., Ma, R., Knowles, D.A., Jafar-Nejad, P., Messing, J., Kim, H.J., Soriano, A., Auburger, G., et al. (2017). Therapeutic reduction of ataxin-2 extends lifespan and reduces pathology in TDP-43 mice. Nature *544*, 367–371.

Bentmann, E., Neumann, M., Tahirovic, S., Rodde, R., Dormann, D., and Haass, C. (2012). Requirements for stress granule recruitment of fused in sarcoma (FUS) and TAR DNA-binding protein of 43 kDa (TDP-43). J. Biol. Chem. *287*, 23079–23094.

Caldecott, K.W. (2014). Protein ADP-ribosylation and the cellular response to DNA strand breaks. DNA Repair (Amst.) *19*, 108–113.

Catara, G., Grimaldi, G., Schembri, L., Spano, D., Turacchio, G., Lo Monte, M., Beccari, A.R., Valente, C., and Corda, D. (2017). PARP1-produced poly-ADP-ribose causes the PARP12 translocation to stress granules and impairment of Golgi complex functions. Sci. Rep. *7*, 14035.

Chang, C.K., Wu, T.H., Wu, C.Y., Chiang, M.H., Toh, E.K., Hsu, Y.C., Lin, K.F., Liao, Y.H., Huang, T.H., and Huang, J.J. (2012). The N-terminus of TDP-43 promotes its oligomerization and enhances DNA binding affinity. Biochem. Biophys. Res. Commun. *425*, 219–224.

Citarelli, M., Teotia, S., and Lamb, R.S. (2010). Evolutionary history of the poly(ADP-ribose) polymerase gene family in eukaryotes. BMC Evol. Biol. *10*, 308.

Cohen, T.J., Hwang, A.W., Unger, T., Trojanowski, J.Q., and Lee, V.M. (2012). Redox signalling directly regulates TDP-43 via cysteine oxidation and disulphide cross-linking. EMBO J. *31*, 1241–1252.

Colombrita, C., Zennaro, E., Fallini, C., Weber, M., Sommacal, A., Buratti, E., Silani, V., and Ratti, A. (2009). TDP-43 is recruited to stress granules in conditions of oxidative insult. J. Neurochem. *111*, 1051–1061.

Combet, C., Blanchet, C., Geourjon, C., and Deléage, G. (2000). NPS@: network protein sequence analysis. Trends Biochem. Sci. *25*, 147–150.

(F) Cells were quantified for the presence of G3BP1-labeled SGs. Mean (± SEM), n = 3, one-way ANOVA ($p < 0.0001$), and Tukey's test.
(G) Cells were quantified for the presence of cytoplasmic TDP-43-GFP foci. Mean (± SEM), n = 3, one-way ANOVA ($p < 0.0001$), and Tukey's test. Asterisks, significant. *$p < 0.05$, **$p < 0.01$, ***$p < 0.001$, and ****$p < 0.0001$.
See Figure S7.

Conicella, A.E., Zerze, G.H., Mittal, J., and Fawzi, N.L. (2016). ALS mutations disrupt phase separation mediated by α-helical structure in the TDP-43 low-complexity C-terminal domain. Structure *24*, 1537–1549.

Dewey, C.M., Cenik, B., Sephton, C.F., Dries, D.R., Mayer, P., 3rd, Good, S.K., Johnson, B.A., Herz, J., and Yu, G. (2011). TDP-43 is directed to stress granules by sorbitol, a novel physiological osmotic and oxidative stressor. Mol. Cell. Biol. *31*, 1098–1108.

Elden, A.C., Kim, H.J., Hart, M.P., Chen-Plotkin, A.S., Johnson, B.S., Fang, X., Armakola, M., Geser, F., Greene, R., Lu, M.M., et al. (2010). Ataxin-2 intermediate-length polyglutamine expansions are associated with increased risk for ALS. Nature *466*, 1069–1075.

Fatokun, A.A., Dawson, V.L., and Dawson, T.M. (2014). Parthanatos: mitochondrial-linked mechanisms and therapeutic opportunities. Br. J. Pharmacol. *171*, 2000–2016.

Gagné, J.P., Hunter, J.M., Labrecque, B., Chabot, B., and Poirier, G.G. (2003). A proteomic approach to the identification of heterogeneous nuclear ribonucleoproteins as a new family of poly(ADP-ribose)-binding proteins. Biochem. J. *371*, 331–340.

Gagné, J.P., Isabelle, M., Lo, K.S., Bourassa, S., Hendzel, M.J., Dawson, V.L., Dawson, T.M., and Poirier, G.G. (2008). Proteome-wide identification of poly(ADP-ribose) binding proteins and poly(ADP-ribose)-associated protein complexes. Nucleic Acids Res. *36*, 6959–6976.

Gagné, J.P., Pic, E., Isabelle, M., Krietsch, J., Ethier, C., Paquet, E., Kelly, I., Boutin, M., Moon, K.M., Foster, L.J., and Poirier, G.G. (2012). Quantitative proteomics profiling of the poly(ADP-ribose)-related response to genotoxic stress. Nucleic Acids Res. *40*, 7788–7805.

Gibson, B.A., and Kraus, W.L. (2012). New insights into the molecular and cellular functions of poly(ADP-ribose) and PARPs. Nat. Rev. Mol. Cell Biol. *13*, 411–424.

Han, T.W., Kato, M., Xie, S., Wu, L.C., Mirzaei, H., Pei, J., Chen, M., Xie, Y., Allen, J., Xiao, G., and McKnight, S.L. (2012). Cell-free formation of RNA granules: bound RNAs identify features and components of cellular assemblies. Cell *149*, 768–779.

Harrison, A.F., and Shorter, J. (2017). RNA-binding proteins with prion-like domains in health and disease. Biochem. J. *474*, 1417–1438.

Hasegawa, M., Arai, T., Nonaka, T., Kametani, F., Yoshida, M., Hashizume, Y., Beach, T.G., Buratti, E., Baralle, F., Morita, M., et al. (2008). Phosphorylated TDP-43 in frontotemporal lobar degeneration and amyotrophic lateral sclerosis. Ann. Neurol. *64*, 60–70.

Hottiger, M.O. (2015). Nuclear ADP-ribosylation and its role in chromatin plasticity, cell differentiation, and epigenetics. Annu. Rev. Biochem. *84*, 227–263.

Hsiao, S.J., and Smith, S. (2008). Tankyrase function at telomeres, spindle poles, and beyond. Biochimie *90*, 83–92.

Huang, S.M., Mishina, Y.M., Liu, S., Cheung, A., Stegmeier, F., Michaud, G.A., Charlat, O., Wiellette, E., Zhang, Y., Wiessner, S., et al. (2009). Tankyrase inhibition stabilizes axin and antagonizes Wnt signalling. Nature *461*, 614–620.

Hyman, A.A., Weber, C.A., and Jülicher, F. (2014). Liquid-liquid phase separation in biology. Annu. Rev. Cell Dev. Biol. *30*, 39–58.

Igaz, L.M., Kwong, L.K., Chen-Plotkin, A., Winton, M.J., Unger, T.L., Xu, Y., Neumann, M., Trojanowski, J.Q., and Lee, V.M. (2009). Expression of TDP-43 C-terminal fragments in vitro recapitulates pathological features of TDP-43 proteinopathies. J. Biol. Chem. *284*, 8516–8524.

Isabelle, M., Gagné, J.P., Gallouzi, I.E., and Poirier, G.G. (2012). Quantitative proteomics and dynamic imaging reveal that G3BP-mediated stress granule assembly is poly(ADP-ribose)-dependent following exposure to MNNG-induced DNA alkylation. J. Cell Sci. *125*, 4555–4566.

Jiang, L.L., Xue, W., Hong, J.Y., Zhang, J.T., Li, M.J., Yu, S.N., He, J.H., and Hu, H.Y. (2017). The N-terminal dimerization is required for TDP-43 splicing activity. Sci. Rep. *7*, 6196.

Johnson, B.S., Snead, D., Lee, J.J., McCaffery, J.M., Shorter, J., and Gitler, A.D. (2009). TDP-43 is intrinsically aggregation-prone, and amyotrophic lateral sclerosis-linked mutations accelerate aggregation and increase toxicity. J. Biol. Chem. *284*, 20329–20339.

Kametani, F., Obi, T., Shishido, T., Akatsu, H., Murayama, S., Saito, Y., Yoshida, M., and Hasegawa, M. (2016). Mass spectrometric analysis of accumulated TDP-43 in amyotrophic lateral sclerosis brains. Sci. Rep. *6*, 23281.

Kato, M., Han, T.W., Xie, S., Shi, K., Du, X., Wu, L.C., Mirzaei, H., Goldsmith, E.J., Longgood, J., Pei, J., et al. (2012). Cell-free formation of RNA granules: low complexity sequence domains form dynamic fibers within hydrogels. Cell *149*, 753–767.

Kedersha, N.L., Gupta, M., Li, W., Miller, I., and Anderson, P. (1999). RNA-binding proteins TIA-1 and TIAR link the phosphorylation of eIF-2 alpha to the assembly of mammalian stress granules. J. Cell Biol. *147*, 1431–1442.

Kedersha, N., Ivanov, P., and Anderson, P. (2013). Stress granules and cell signaling: more than just a passing phase? Trends Biochem. Sci. *38*, 494–506.

Kim, H.J., Raphael, A.R., LaDow, E.S., McGurk, L., Weber, R.A., Trojanowski, J.Q., Lee, V.M., Finkbeiner, S., Gitler, A.D., and Bonini, N.M. (2014). Therapeutic modulation of eIF2α phosphorylation rescues TDP-43 toxicity in amyotrophic lateral sclerosis disease models. Nat. Genet. *46*, 152–160.

Krietsch, J., Rouleau, M., Pic, É., Ethier, C., Dawson, T.M., Dawson, V.L., Masson, J.Y., Poirier, G.G., and Gagné, J.P. (2013). Reprogramming cellular events by poly(ADP-ribose)-binding proteins. Mol. Aspects Med. *34*, 1066–1087.

Leung, A.K. (2014). Poly(ADP-ribose): an organizer of cellular architecture. J. Cell Biol. *205*, 613–619.

Leung, A.K., Vyas, S., Rood, J.E., Bhutkar, A., Sharp, P.A., and Chang, P. (2011). Poly(ADP-ribose) regulates stress responses and microRNA activity in the cytoplasm. Mol. Cell *42*, 489–499.

Li, Y.R., King, O.D., Shorter, J., and Gitler, A.D. (2013). Stress granules as crucibles of ALS pathogenesis. J. Cell Biol. *201*, 361–372.

Lin, Y., Protter, D.S., Rosen, M.K., and Parker, R. (2015). Formation and Maturation of Phase-Separated Liquid Droplets by RNA-Binding Proteins. Mol. Cell *60*, 208–219.

Ling, S.C., Albuquerque, C.P., Han, J.S., Lagier-Tourenne, C., Tokunaga, S., Zhou, H., and Cleveland, D.W. (2010). ALS-associated mutations in TDP-43 increase its stability and promote TDP-43 complexes with FUS/TLS. Proc. Natl. Acad. Sci. USA *107*, 13318–13323.

Liu-Yesucevitz, L., Bilgutay, A., Zhang, Y.J., Vanderweyde, T., Citro, A., Mehta, T., Zaarur, N., McKee, A., Bowser, R., Sherman, M., et al. (2010). Tar DNA binding protein-43 (TDP-43) associates with stress granules: analysis of cultured cells and pathological brain tissue. PLoS ONE *5*, e13250.

Mackenzie, I.R., Bigio, E.H., Ince, P.G., Geser, F., Neumann, M., Cairns, N.J., Kwong, L.K., Forman, M.S., Ravits, J., Stewart, H., et al. (2007). Pathological TDP-43 distinguishes sporadic amyotrophic lateral sclerosis from amyotrophic lateral sclerosis with SOD1 mutations. Ann. Neurol. *61*, 427–434.

Mackenzie, I.R., Nicholson, A.M., Sarkar, M., Messing, J., Purice, M.D., Pottier, C., Annu, K., Baker, M., Perkerson, R.B., Kurti, A., et al. (2017). TIA1 Mutations in amyotrophic lateral sclerosis and frontotemporal dementia promote phase separation and alter stress granule dynamics. Neuron *95*, 808–816.e9.

Mariotti, L., Pollock, K., and Guettler, S. (2017). Regulation of Wnt/β-catenin signalling by tankyrase-dependent poly(ADP-ribosyl)ation and scaffolding. Br. J. Pharmacol. *174*, 4611–4636.

McGurk, L., Lee, V.M., Trojanowksi, J.Q., Van Deerlin, V.M., Lee, E.B., and Bonini, N.M. (2014). Poly-A binding protein-1 localization to a subset of TDP-43 inclusions in amyotrophic lateral sclerosis occurs more frequently in patients harboring an expansion in C9orf72. J. Neuropathol. Exp. Neurol. *73*, 837–845.

Mojsilovic-Petrovic, J., Jeong, G.B., Crocker, A., Arneja, A., David, S., Russell, D.S., and Kalb, R.G. (2006). Protecting motor neurons from toxic insult by antagonism of adenosine A2a and Trk receptors. J. Neurosci. *26*, 9250–9263.

Molliex, A., Temirov, J., Lee, J., Coughlin, M., Kanagaraj, A.P., Kim, H.J., Mittag, T., and Taylor, J.P. (2015). Phase separation by low complexity domains promotes stress granule assembly and drives pathological fibrillization. Cell *163*, 123–133.

Mompeán, M., Romano, V., Pantoja-Uceda, D., Stuani, C., Baralle, F.E., Buratti, E., and Laurents, D.V. (2016). The TDP-43 N-terminal domain structure at high resolution. FEBS J. *283*, 1242–1260.

Murakami, T., Qamar, S., Lin, J.Q., Schierle, G.S., Rees, E., Miyashita, A., Costa, A.R., Dodd, R.B., Chan, F.T., Michel, C.H., et al. (2015). ALS/FTD mutation-induced phase transition of FUS liquid droplets and reversible hydrogels into irreversible hydrogels impairs RNP granule function. Neuron *88*, 678–690.

Neumann, M., Sampathu, D.M., Kwong, L.K., Truax, A.C., Micsenyi, M.C., Chou, T.T., Bruce, J., Schuck, T., Grossman, M., Clark, C.M., et al. (2006). Ubiquitinated TDP-43 in frontotemporal lobar degeneration and amyotrophic lateral sclerosis. Science *314*, 130–133.

Neumann, M., Kwong, L.K., Lee, E.B., Kremmer, E., Flatley, A., Xu, Y., Forman, M.S., Troost, D., Kretzschmar, H.A., Trojanowski, J.Q., and Lee, V.M. (2009). Phosphorylation of S409/410 of TDP-43 is a consistent feature in all sporadic and familial forms of TDP-43 proteinopathies. Acta Neuropathol. *117*, 137–149.

Nonaka, T., Arai, T., Buratti, E., Baralle, F.E., Akiyama, H., and Hasegawa, M. (2009). Phosphorylated and ubiquitinated TDP-43 pathological inclusions in ALS and FTLD-U are recapitulated in SH-SY5Y cells. FEBS Lett. *583*, 394–400.

Panzeter, P.L., Zweifel, B., Malanga, M., Waser, S.H., Richard, M., and Althaus, F.R. (1993). Targeting of histone tails by poly(ADP-ribose). J. Biol. Chem. *268*, 17662–17664.

Patel, A., Lee, H.O., Jawerth, L., Maharana, S., Jahnel, M., Hein, M.Y., Stoynov, S., Mahamid, J., Saha, S., Franzmann, T.M., et al. (2015). A liquid-to-solid phase transition of the ALS protein FUS accelerated by disease mutation. Cell *162*, 1066–1077.

Pleschke, J.M., Kleczkowska, H.E., Strohm, M., and Althaus, F.R. (2000). Poly(ADP-ribose) binds to specific domains in DNA damage checkpoint proteins. J. Biol. Chem. *275*, 40974–40980.

Romano, V., Quadri, Z., Baralle, F.E., and Buratti, E. (2015). The structural integrity of TDP-43 N-terminus is required for efficient aggregate entrapment and consequent loss of protein function. Prion *9*, 1–9.

Rueden, C.T., Schindelin, J., Hiner, M.C., DeZonia, B.E., Walter, A.E., Arena, E.T., and Eliceiri, K.W. (2017). ImageJ2: ImageJ for the next generation of scientific image data. BMC Bioinformatics *18*, 529.

Ryan, V.H., Dignon, G.L., Zerze, G.H., Chabata, C.V., Silva, R., Conicella, A.E., Amaya, J., Burke, K.A., Mittal, J., and Fawzi, N.L. (2018). Mechanistic view of hnRNPA2 low-complexity domain structure, interactions, and phase separation altered by mutation and arginine methylation. Mol. Cell *69*, 465–479.e7.

Schultheisz, H.L., Szymczyna, B.R., and Williamson, J.R. (2009). Enzymatic synthesis and structural characterization of 13C, 15N-poly(ADP-ribose). J. Am. Chem. Soc. *131*, 14571–14578.

Shah, G.M., Poirier, D., Duchaine, C., Brochu, G., Desnoyers, S., Lagueux, J., Verreault, A., Hoflack, J.C., Kirkland, J.B., and Poirier, G.G. (1995). Methods for biochemical study of poly(ADP-ribose) metabolism in vitro and in vivo. Anal. Biochem. *227*, 1–13.

Smith, S., Giriat, I., Schmitt, A., and de Lange, T. (1998). Tankyrase, a poly(ADP-ribose) polymerase at human telomeres. Science *282*, 1484–1487.

Sun, Z., Diaz, Z., Fang, X., Hart, M.P., Chesi, A., Shorter, J., and Gitler, A.D. (2011). Molecular determinants and genetic modifiers of aggregation and toxicity for the ALS disease protein FUS/TLS. PLoS Biol. *9*, e1000614.

Teloni, F., and Altmeyer, M. (2016). Readers of poly(ADP-ribose): designed to be fit for purpose. Nucleic Acids Res. *44*, 993–1006.

Voronkov, A., Holsworth, D.D., Waaler, J., Wilson, S.R., Ekblad, B., Perdreau-Dahl, H., Dinh, H., Drewes, G., Hopf, C., Morth, J.P., and Krauss, S. (2013). Structural basis and SAR for G007-LK, a lead stage 1,2,4-triazole based specific tankyrase 1/2 inhibitor. J. Med. Chem. *56*, 3012–3023.

Wang, A., Conicella, A.E., Schmidt, H.B., Martin, E.W., Rhoads, S.N., Reeb, A.N., Nourse, A., Ramirez Montero, D., Ryan, V.H., Rohatgi, R., et al. (2018). A single N-terminal phosphomimic disrupts TDP-43 polymerization, phase separation, and RNA splicing. EMBO J. *37*, e97452.

Winton, M.J., Igaz, L.M., Wong, M.M., Kwong, L.K., Trojanowski, J.Q., and Lee, V.M. (2008). Disturbance of nuclear and cytoplasmic TAR DNA-binding protein (TDP-43) induces disease-like redistribution, sequestration, and aggregate formation. J. Biol. Chem. *283*, 13302–13309.

Wippich, F., Bodenmiller, B., Trajkovska, M.G., Wanka, S., Aebersold, R., and Pelkmans, L. (2013). Dual specificity kinase DYRK3 couples stress granule condensation/dissolution to mTORC1 signaling. Cell *152*, 791–805.

Wittmann, C.W., Wszolek, M.F., Shulman, J.M., Salvaterra, P.M., Lewis, J., Hutton, M., and Feany, M.B. (2001). Tauopathy in Drosophila: neurodegeneration without neurofibrillary tangles. Science *293*, 711–714.

Xiang, S., Kato, M., Wu, L.C., Lin, Y., Ding, M., Zhang, Y., Yu, Y., and McKnight, S.L. (2015). The LC domain of hnRNPA2 adopts similar conformations in hydrogel polymers, liquid-like droplets, and nuclei. Cell *163*, 829–839.

Xiao, S., Sanelli, T., Chiang, H., Sun, Y., Chakrabartty, A., Keith, J., Rogaeva, E., Zinman, L., and Robertson, J. (2015). Low molecular weight species of TDP-43 generated by abnormal splicing form inclusions in amyotrophic lateral sclerosis and result in motor neuron death. Acta Neuropathol. *130*, 49–61.

Zhang, Y.J., Caulfield, T., Xu, Y.F., Gendron, T.F., Hubbard, J., Stetler, C., Sasaguri, H., Whitelaw, E.C., Cai, S., Lee, W.C., and Petrucelli, L. (2013). The dual functions of the extreme N-terminus of TDP-43 in regulating its biological activity and inclusion formation. Hum. Mol. Genet. *22*, 3112–3122.

Zhang, K., Daigle, J.G., Cunningham, K.M., Coyne, A.N., Ruan, K., Grima, J.C., Bowen, K.E., Wadhwa, H., Yang, P., Rigo, F., et al. (2018). Stress granule assembly disrupts nucleocytoplasmic transport. Cell *173*, 958–971.e17.

STAR★METHODS

KEY RESOURCES TABLE

REAGENT or RESOURCE	SOURCE	IDENTIFIER
Antibodies		
Mouse anti-Ataxin-2	BD Biosciences	Cat# 611378; RRID:AB_398900
Goat anti-eIF3	Santa Cruz Biotechnology	Cat# sc-16377; RRID:AB_671941
Mouse anti-eIF3	Santa Cruz Biotechnology	Cat# sc-137214; RRID:AB_2277705
Mouse anti-β-galactosidase	Promega	Cat# Z378A; RRID:AB_2313752
Rabbit anti-G3BP1	ThermoFisher Scientific	Cat# PA5-29455; RRID:AB_2546931
Mouse anti-LaminC	DSHB	Cat# lc28.26; RRID:AB_528339
Mouse anti-PAR (BSA free)	Tulip Biolabs	Cat # 1020/N RRID; N/A
Mouse anti-PAR	Enzo life sciences	Cat # BML-SA216 RRID: N/A
Rabbit anti-PAR LP-96 (discontinued)	BD Biosciences	Cat# 551813; RRID:AB_394263
Mouse anti-pS409/10	Cosmo Bio USA	TIP-PTD-MO1 RRID: N/A
Rabbit anti-pS409/10	Cosmo Bio USA	TIP-PTD-PO1 RRID: N/A
Rabbit anti-TDP-43	Proteintech Group	Cat# 10782-2-AP; RRID:AB_615042
Mouse anti-TIAR	BD Biosciences	BD Biosciences Cat# 610352; RRID:AB_397742
Rabbit anti-β-Tubulin-HRP	Cell signaling	Cat# 9099S; RRID:AB_10695471
Goat anti-rabbit-HRP	Millipore	Cat# AP307P; RRID:AB_11212848
Goat anti-mouse-HRP	Abcam	Cat# ab6789; RRID:AB_955439
Goat anti-mouse-HRP	Jackson ImmunoResearch Laboratories	Cat# 115-035-146; RRID:AB_2307392
Donkey anti-mouse-AF488		Cat # A-21202; RRID:AB_141607
Rabbit anti-goat-AF488	ThermoFisher Scientific	Cat# A-11078; RRID:AB_141838
Donkey anti-mouse-AF568	ThermoFisher Scientific	Cat# A10037; RRID:AB_2534013
Donkey anti-mouse-AF594	ThermoFisher Scientific	Cat# A-21203; RRID:AB_141633
Goat anti-mouse-AF647	ThermoFisher Scientific	Cat# A-21236; RRID:AB_141725
Goat anti-rabbit-AF594	ThermoFisher Scientific	Cat# A-11012; RRID:AB_141359
Goat anti-rabbit-AF568	ThermoFisher Scientific	Cat# A-11036; RRID:AB_10563566
Goat anti-rabbit-AF647	ThermoFisher Scientific	Cat# A-21245; RRID:AB_2535813
Bacterial and Virus Strains		
E. coli BL21 DE3 (RIL) cells	Agilent	Cat# 230245; RRID: N/A
Chemicals, Peptides, and Recombinant Proteins		
ADP-HPD	EMD Millipore	Cat# 118415-1SET; RRID: N/A
Bouin's solution	Sigma Aldrich	Cat# HT10132-1L; RRID: N/A
Cytoseal XYL	Thermo Fisher Scientific	Cat# 8312-16E; RRID: N/A
dPBS with calcium and magnesium	Thermo Fisher Scientific	Cat # 14040133; RRID; N/A
dPBS no calcium no magnesium	Thermo Fisher Scientific	Cat# 14190250; RRID: N/A
Fetal bovine serum	Sigma Aldrich	Cat# F6178-500ML; RRID: N/A
G007-LK	SelleckChem	Cat# 1380672-07-0; RRID: N/A
Histoclear	National diagnostics	Cat# HS-200 RRID; N/A
Hoescht 3342	ThermoFisher Scientific	Cat# H3570; RRID: N/A
IWR-1-endo	SelleckChem	Cat# 1127442-82-3; RRID: N/A
Poly(ADP-ribose) free polymer	TREVIGEN	Cat# 4336-100-01; RRID: N/A
Paraformaldehyde	Electron Microscopy Sciences	Cat# 15713; RRID: N/A
Penicillin-streptomycin	Thermo Fisher Scientific	Cat# 15140122; RRID: N/A

(*Continued on next page*)

Continued

REAGENT or RESOURCE	SOURCE	IDENTIFIER
Pierce IP Lysis buffer	Thermo Fisher Scientific	Cat# 87787; RRID: N/A
sodium arsenite	Sigma Aldrich	Cat #35000 1L-R; RRID#: N/A
sodium periodate	Sigma Aldrich	Cat#: 311448-5G; RRID#: N/A
succinic dihydrazide	Sigma Aldrich	Cat#: S5502-25G; RRID#: N/A
SYPRO Ruby	Thermo Fisher Scientific	Cat #S1200; RRID#: N/A
Trizol	ThermoFisher Scientific	Cat# 15596026; RRID: N/A
XAV939	SelleckChem	Cat# S1180; RRID: N/A
$NLS_{71\text{-}90}$ LVYVVNYPKDNKRKMDETDA	GenScript	N/A
$NLS_{91\text{-}110}$ SSAVKVKRAVQKTSDLIVLG	GenScript	N/A
$MMRP_{172\text{-}156}$ KKKKKRFSFKKSFKLSGFSFKKNKK	GenScript	N/A
$MMRP_{152\text{-}176\text{-}mut}$ AAAAAAASAKKSAKASGASAKKNKK	GenScript	N/A
Human GST-TDP-43	This paper	N/A
Human GST-TDP-43-PBM1	This paper	N/A
Human GST-TDP-43-PBM2	This paper	N/A
Human GST-TDP-43-ΔPBM	This paper	N/A
His_6-SUMO-TDP-43-WT	This paper	N/A
His_6-SUMO-TDP-43- ΔPBM	This paper	N/A
His_6-SUMO-TDP-43-C35	This paper	N/A
His_6-SUMO-TDP-43-C25	This paper	N/A
His_6-SUMO-TDP-43-Q331K	This paper	N/A
Critical Commercial Assays		
ECL prime	Amersham	Cat# RPN2236 RRID: N/A
ECL Western Blotting Analysis System	Amersham	Cat# RPN2109 RRID: N/A
Fast SYBR Green	ThermoFisher Scientific	Cat# 4385612 RRID: N/A
lipofectamine 2000	Thermo Fisher Scientific	Cat# 11668027 RRID: N/A
lipofectamine LTX	Thermo Fisher Scientific	Cat# 15338100
NER-PER nuclear and cytoplasmic extraction kit	ThermoFisher Scientific	Cat # 78833 RRID: N/A
Pierce co-immunoprecipitation kit	ThermoFisher Scientific	Cat# 26149 RRID: N/A
Pierce Antibody Clean-up Kit	ThermoFisher Scientific	Cat# 44600 RRID: N/A
Superscript III	ThermoFisher Scientific	Cat# 18080093 RRID: N/A
QuikChange XL Site-Directed Mutagenesis Kit	Agilent Technologies	Cat#: 200517; RRID#: N/A
TURBO DNase	ThermoFisher Scientific	Cat# AM2238 RRID: N/A
Experimental Models: Cell Lines		
COS-7 cells: African green monkey kidney fibroblast-like cell line	ATCC	Cat# CRL-1651; RRID:CVCL_0224
Experimental Models: Organisms/Strains		
Drosophila: UAS-TDP-43 (37M)/CyO; gmr-GAL4(YH3)/TM6B	Elden et al., 2010; Kim et al., 2014	N/A
Drosophila: *Elav3A-GAL4, UAS-TDP43/TM6B*	Elden et al., 2010; Kim et al., 2014	N/A
Drosophila: UAS-Tau R406W	Wittmann et al., 2001	N/A
Drosophila: *P{w[+mC] = GAL4-elav.L}2/CyO*	Bloomington Stock Center	BDSC Cat# 8760; RRID:BDSC_8760
Drosophila: y^1 *w*; P{UAS-mCD8::GFP.L}2)*	Bloomington Stock Center	BDSC Cat# 5137; RRID:BDSC_5137
Drosophila: w^{1118}	Bloomington Stock Center	BDSC Cat# 5905; RRID:BDSC_5905
w[1118]; P{w[+mC] = EPg}Tnks[HP37069]	Bloomington Stock Center	BDSC Cat# 22129; RRID:BDSC_22129
w[1118]; P{w[+mC] = EP}Tnks[EP3476]/TM6B, Tb[1]	Bloomington Stock Center	BDSC Cat# 17132; RRID:BDSC_17132
Drosophila: w[1118], +/+; daugtherless-GAL4 (*da-GAL4*)	Bloomington stock center	BDSC Cat# 5581; RRID:BDSC_5581
Drosophila: *w*; UAS-Tnks. IR*$^{4179R\text{-}4}$*/Cy*	Fly Stocks of National Institute of Genetics (NIG-Fly)	NIG-Fly Cat#: 4179R-4; RRID: N/A

(*Continued on next page*)

Continued

REAGENT or RESOURCE	SOURCE	IDENTIFIER
Oligonucleotides		
PBM1:5′GTTGTCAACTATCCAAAAGATAACGCAGCAGCA ATGGATGAGACAGATGCT 3′	IDT oligo	N/A
PBM2: 5′GATGCTTCATCAGCAGTGGCAGTGGCAGCAGC AGTCCAGAAAACATCGAT 3′	IDT oligo	N/A
Q331K:5′ CGCCCAGGCAGCACTAATGAGCAGTTGGGG 3′	IDT oligo	N/A
Tankyrase RT FP: 5′ ATCTCTGCGCATACCAGCTT 3′	IDT oligo	N/A
Tankyrase RT RP: 5′ ATCTCTGCGCATACCAGCTT 3′	IDT oligo	N/A
beta-tubulin FP: 5′CATCCAAGCTGGTCAGTG 3′	IDT oligo	N/A
beta-tubulin RP: 5′ GCCATGCTCATCGGAGAT 3′	IDT oligo	N/A
Recombinant DNA		
Human TDP-43 in pDuet-GST	Johnson et al., 2009	N/A
Human TDP-43-PBM1 in pDuet-GST	This paper	N/A
Human TDP-43-PBM2 in pDuet-GST	This paper	N/A
Human TDP-43-ΔPBM in pDuet-GST	This paper	N/A
Human TDP-43-WT-YFP cloned in to pcDNA3	Elden et al., 2010	N/A
Human TDP-43-ΔPBM-YFP cloned in to pcDNA3.	This paper	N/A
Human TDP-43-PBM1-YFP cloned in to pcDNA3.	This paper	N/A
Human TDP-43-ΔPBM-GFP in pcDNA3-C-eGFP	This paper/ GenScript	N/A
pE-SUMO	LifeSensors	N/A
TDP-43-WT in pE-SUMO	This paper	N/A
TDP-43-ΔPBM in pE-SUMO	This paper	N/A
TDP-43-C35 (amino acids 85-414) in pE-SUMO	This paper	N/A
TDP-43-Q331K (amino acids 176-414) in pE-SUMO	This paper	N/A
TDP-43-WT in pcDNA3-C-eGFP	This paper/GenScript	N/A
TDP-43-ΔPBM in pcDNA3-C-eGFP	This paper/GenScript	N/A
TDP-43-C35 (amino acids 85-414) in pcDNA3-C-eGFP	This paper/GenScript	N/A
TDP-43-C25 (amino acids 176-414) in pcDNA3-C-eGFP	This paper/GenScript	N/A
TDP-43-ΔPBM-$_{PBM-A2/B1}$ in pcDNA3-C-eGFP	This paper/GenScript	N/A
TDP-43-MBP-His_6 in PJ4M/TDP-43	Wang et al., 2018	ADDGENE #104480; RRID: N/A
Software and Algorithms		
Prism 6	GraphPad	N/A
ImageJ	Rueden et al., 2017	N/A

CONTACT FOR REAGENT AND RESOURCE SHARING

Requests for resources, reagents and further information should be directed to, and will be fulfilled by, Nancy M. Bonini (nbonini@sas.upenn.edu).

EXPERIMENTAL MODEL AND SUBJECT DETAILS

Drosophila stocks and maintenance

All *Drosophila* stocks are described in the Key Resources Table. Briefly, transgenic lines for TDP-43 were described previously (Elden et al., 2010; Kim et al., 2014). The RNAi line to *tankyrase* (4179R-4) was obtained from the Fly Stocks of National Institute of Genetics (NIG-Fly), Kyoto, Japan. *UAS-mCD8-GFP* (y^1 w^*; *UAS-mCD8:GFP.L*) obtained from the Bloomington stock center was backcrossed, six times, to w^{1118} line isogenic for chromosomes 1, 2 and 3 (*5905*). *UAS-hTau R406W* (Wittmann et al., 2001) was a kind gift from a gift of M. Feany (Harvard Medical School, Boston, MA, USA). All other stocks were obtained from the Bloomington *Drosophila* stock center, Indiana, USA. All fly experiments were carried out at 25°C in standard cornmeal molasses agar.

Mammalian cells and culture details

COS-7 cells were originally purchased by ATCC and were kindly provided by Virginia M. Lee, University of Pennsylvania. Cells were authenticated by ATCC before purchase. The cell lines were not tested for mycoplasma contamination. No commonly misidentified cell lines were used. Cells were routinely cultured in Dulbecco's modified Eagle's medium (DMEM) with high glucose supplemented with 10% fetal bovine serum and 1% penicillin-streptomycin. Cells were grown at 37°C with 5% CO_2, and a water bath was used for humidification. Cells were washed with Dulbeccos PBS without calcium and without magnesium and trypsinized in Trypsin with 0.25% EDTA (ThermoFisher Scientific).

Rat cortical neuron cultures

Studies were approved by the Children's Hospital of Pennsylvania Institutional Animal Care and Use Committee (CHOP IACUC), the assigned protocol number was 594. All studies adhered to all regulatory standards. Rat cortical neuron cultures were prepared from embryos isolated from female Sprague Dawley wild rats that were 16-18 days pregnant. Neurons were cultured as previously described (Mojsilovic-Petrovic et al., 2006). Briefly, tissue was dissociated with 5% trypsin and 1mg/ml DNase, cells were cultured in 12-well plates in conditioned neuralbasal medium with serum-free B-27 (ThermoFisher Scientific) and penicillin-streptomycin (ThermoFisher Scientific). After 3-4 days *in vitro* (DIV) cell division was stopped by the addition of 5 μM cytosine arabinoside (AraC) (Sigma-Aldrich). Cells were maintained in preconditioned neuralbasal medium with serum-free B-27 (ThermoFisher Scientific) and penicillin-streptomycin (ThermoFisher Scientific).

METHOD DETAILS

Drosophila external eye imaging and histology

External eyes and internal retinas were imaged in female flies aged 2-3d. For quantification, the integrity of the external eye was scored in ten female flies from three independent crosses for each genotype. Control and experimental crosses were propagated at the same time and incubated in the same incubator (25°C). The internal retina was quantified using imageJ (Rueden et al., 2017) from paraffin sections at the same anatomical position for all animals. Three sections per animal were imaged and quantified, this was repeated on 3-5 female heads from each genotype.

Drosophila lifespan

For lifespan analysis, more than 190 males (1d-old) for each genotype were separated into groups of 15-20 and aged in vials containing fresh standard cornmeal molasses agar. Every second day dead flies were scored and the survivors were tipped into a fresh food vial. Kaplan-Meir survival curves were plotted and a log-rank test for trend was performed using Graphpad prism 6. The lifespan analysis was repeated three independent times at different times throughout the year.

Nuclear Cytoplasmic fractionation

The NER-PER nuclear and cytoplasmic extraction reagents (Thermo Scientific) was used to fractionate the nuclear and cytoplasmic protein from fly heads. The instructions were followed with the following modifications: 10 male heads were homogenized in 110 μL of ice-cold CERI for 1 minute, the sample was vortexed on the highest setting for 30 s to fully suspend the cell pellet. The sample was incubated the on ice for 10 min and then 5.5 μL of ice-cold CER II was added. The sample was vortexed for 10 s on the highest setting, and then incubated on ice for 2 mins. The sample was vortexed on the highest setting for 15 s and then centrifuged at maximum speed for 10 mins at 4°C. The supernatant (cytoplasmic extract) was immediately transferred to a clean pre-chilled tube. The supernatant was spun again at maximum speed for 10 min at 4°C, the supernatant (cytoplasmic extract) was transferred to a pre-chilled tube. The nuclear pellet was washed in 50 μL of ice-cold CERI, and then centrifuged at maximum speed for 10 min at 4°C. The supernatant was discarded and the pellet was resuspended in 55 μL of ice-cold NER. The samples were vortexed on the highest setting for 10 s every 10 min for a total of 40 mins. The samples were centrifuged at maximum speed for 10 mins at 4°C. The supernatant (nuclear fraction was transferred to pre-chilled tube. Samples for immunoblotting were made up in 1X LDS loading buffer, with 5% β-mercaptoethanol, heat denatured at 95°C, chilled for 5 min and centrifuged at 5000 rpm for 5 mins at 4°C. For the total protein immunoblots that correspond to the nuclear and cytoplasmic fractionation, 10 male heads were homogenized in 100 μL Laemelli buffer with β-mercaptoethanol, heat denatured at 95°C, chilled for 5 min and centrifuged at 5000 rpm for 5 mins at 4°C. The equivalent of half of a fly head was loaded into each well for each sample type (nuclear, cytoplasmic and total). Protein was electrophoresed on 4%–12% Bis-Trsi gel and transferred onto nitrocellulose by wet transfer (20 volts for 75 mins). Blots were blocked in 5% milk in TBS supplemented with 0.05% TWEEN®20 pH 8 (TBST). Primaries made up in TBST were rabbit anti-TDP-43 (1 in 3000, Proteintech), then mouse anti-Lamin A/C (1 in 1000, DSHB) and then anti-tubulin-HRP (1 in 1,000; Cell Signaling Technology). TDP-43 was always detected first, tubulin, migrates closely to TDP-43, and will interfere with TDP-43 signal detection. Secondary antibodies made up in TBST were anti-mouse HRP (1 in 5000, abcam) and anti-Rabbit-HRP (1 in 5000, EMD Millipore). TDP-43 was detected with ECL (GE healthcare Bio-Sciences) and Tubulin and Lamin A/C were detected with ECL Prime (GE Healthcare Bio-Sciences). Quantification of protein blots was performed using ImageJ software (Rueden et al., 2017). All experiments were carried out on three or more biological replicates and statistical analysis was carried out using prism 6 software.

Immunoblotting of *Drosophila* total protein

For experiments where the transgene (TDP-43 or LacZ) was expressed in the eye with *gmr-GAL4*, protein was extracted from 10 female heads in 100 μL of 2X Laemelli buffer with 5% (v/v) β-mercaptoethanol, heat denatured at 95°C, chilled on ice for 5 mins and centrifuged at 5000 rpm for 5 mins at 4°C. The equivalent of half of a fly head was loaded into each well of a 4%–12% Bis-Tris gel and transferred onto nitrocellulose by wet transfer (20 V for 75 mins). Blots were blocked in 5% milk in TBST (TBS supplemented with 0.05% TWEEN®20 pH 8.0). Primary antibodies made up in TBST were: TDP-43 (1 in 3000; Proteintech), α-Tubulin-HRP (1 in 1,000; Cell Signaling Technology) and β−galactosidase (1 in 1,000; Promega). HRP-coupled secondary antibodies used: goat antibody to rabbit (1 in 5,000; EMD Millipore) and goat antibody to mouse (1 in 2,000; Jackson ImmunoResearch Laboratories, Inc.). All experiments were carried out on three or more biological replicates, blots were quantified with ImageJ (Rueden et al., 2017) and statistical analysis was carried out using Graphpad prism 6 software.

Real-time PCR

20 third instar larvae from each genotype were homogenized in 250 μl of Trizol. A further 250 μL of Trizol and 100 μl of chloroform was added and the tube was vigorously shaken for 15 s at room temperature. The samples were centrifuged at maximum speed for 10 min at 4°C and the upper-aqueous phase was transferred to a fresh and pre-chilled tube. The chloroform extraction was repeated on the aqueous phase. RNA was precipitated in 2 volumes of 100% ethanol and 1/10th the volume of 3 M sodium acetate pH 5.2, and the RNA sample was left on ice for 25 mins. The samples were then centrifuged at maximum speed at 4°C for 10 mins. The RNA pellet was washed in 70% ethanol and centrifuged at maximum speed at 4°C for 10 mins. The pellet was air-dried and the RNA was dissolved in 40 μL of DEPC-treated water. Genomic DNA in half of the RNA sample was digested with turbo DNase (Ambion) using the vigorous protocol. 500 ng of RNA was used for first-strand DNA synthesis by Superscript III (ThermoFisher Scientific) with random primers. Fast SYBR Green (ThermoFisher Scientific) was used for real-time analysis. Standard curves were used to test the efficiency of all the primers and to determine the amount of cDNA to add to the PCR reaction. Each experiment was carried out on larvae prepared from 4 independent fly crosses. Statistics were calculated using Graphpad prism 6 software. Primers used were:

Tankyrase RT FP: 5′ ATCTCTGCGCATACCAGCTT 3′
Tankyrase RT RP: 5′ ATCTCTGCGCATACCAGCTT 3′
beta-tubulin FP: 5′CATCCAAGCTGGTCAGTG 3′
beta-tubulin RP: 5′ GCCATGCTCATCGGAGAT 3′

Co-immunoprecipitation

To co-immunoprecipitate PARylated protein and TDP-43 from male fly heads the Pierce co-immunoprecipitation kit (ThermoFisher Scientific) was used according to the manufacturer's instructions. Briefly, 100 μL (1mg/ml) of anti-PAR (clone 10H, BSA free, Tulip Biolabs) was diluted in 100 μL of PBS and desalted using 2ml Zeba desalting columns (Thermo scientific). 33 μg of desalted antibody was immobilized to the agarose resin. Adult male flies, expressing TDP-43 with *elav-GAL4*, were aged to day 4, a total of no more than 22 heads were homogenized for 1 min on ice in 200 μL of IP Lysis/wash buffer (Thermo Scientific), that was supplemented with cOmplete Mini EDTA-free inhibitor (Roche) and ADP-HPD (Calbiochem) at a final concentration of 1 μM. A total of 20 μL was removed for input. Samples were pre-cleared with agarose (1 hr with gentle shaking at 4°C). Precleared lysate was incubated with the antibody-agarose resin at 4°C for 14 hrs, then washed 3 times in lysis buffer containing protease inhibitor and 1 μM ADP-HPD (10 mins each with rotation at 4°C), and eluted in 50 μL of elution buffer. Samples for immunoblotting were prepared in 1X LDS sample buffer, heat denatured at 90°C for 6 min and electrophoresed on a NuPAGE 4%–12% Bis-Tris gel. TDP-43 was detected using anti-TDP-43 (1 in 250; Proteintech) and ECL Prime (GE Healthcare Bio-Sciences).

COS-7 cells were lysed in IP Lysis buffer (Thermo Scientific) containing 1 μM ADP-HPD (Calbiochem) and cOmplete Mini EDTA-free inhibitor (Roche). Lysate was removed for input analysis and the remaining cell lysate was pre-cleared in either Agarose-G or dynabeads^{TM} protein G (both ThermoFisher Scientific) for 1 hr at 4°C. 5 μg of anti-TDP-43 (Proteintech), 5 μg of anti-PAR (10H) BSA free (Tulip Biolabs) and 5 μg of anti-PAR (Enzo life sciences) were coupled to 50 μl of Agarose-G or dynabeads^{TM} protein G and incubated with the precleared lysate. The beads were washed once in lysis buffer, once in lysis buffer supplemented with 300 mM NaCl, and once more in lysis buffer (each 10 min with rotation at 4°C). Beads were denatured at 70°C for 10 min in 1X LDS buffer and electrophoresed on a NuPAGE 4%–12% Bis-Tris gel. Antibodies used for detection were rabbit anti-TDP-43 (1 in 3000; Proteintech), rabbit anti-PAR LP-96 (1 in 500; BD Biosciences). HRP-coupled secondary antibodies used: goat antibody to rabbit (1 in 5,000; EMD Millipore) and goat antibody to mouse (1 in 2,000; Jackson ImmunoResearch Laboratories, Inc.).

Plasmids

Human TDP-43 in pDuet-GST was previously described (Johnson et al., 2009). Human TDP-43-WT-YFP cloned in to pcDNA3.2 was described previously (Elden et al., 2010). Full-length human TDP-43, TDP-43-C35 (amino acids 85-414) and TDP-43-C25 (amino acids 176-414) were subcloned into pE-SUMO (LifeSensors).

TDP-43-WT, TDP-43-ΔPBM, TDP-43-C35 (amino acids 85-414) and TDP-43-C25 (amino acids 176-414) were subcloned into pcDNA3-C-eGFP by GenScript. TDP-43-MBP-His_6 in PJ4M/TDP-43, obtained from ADDGENE, was described previously (Wang et al., 2018). PBM1 and PBM2 mutations were generated in TDP-43-WT-YFP (pcDNA3.2), GST-TDP-43-WT (pDuet-GST) and SUMO-TDP-43-WT (pE-SUMO) by performing site directed mutagenesis (QuikChange II XL) using the following primers:

PBM1: 5′GTTGTCAACTATCCAAAAGATAACGCAGCAGCAATGGATGAGACAGATGCT 3′
PBM2: 5′GATGCTTCATCAGCAGTGGCAGTGGCAGCAGCAGTCCAGAAAACATCGAT 3′

The Q331K mutation in TDP-43-WT (pE-SUMO) was generated by site directed mutagenesis (QuikChange II XL) using the following primer:

Q331K: 5'' CGCCCAGGCAGCACTAATGAGCAGTTGGGG 3′

The DNA sequence corresponding to the hnRNPA1/B2 peptide, was cloned immediately upstream of the stop site in TDP-43-ΔPBM in pcDNA3-C-eGFP, by GenScript, to create TDP-43ΔPBM-$_{PBM-A2/B1}$. The DNA sequence subcloned was:

5′AGAGAGGAATCTGGAAAACCAGGGGCTCATGTAACTGTGAAGAAGCTGTTTGTTGGCGGAATTAAA 3′

All plasmid inserts were sequenced and confirmed to be free of any errors.

Cell stress assays and immunofluorescence

COS-7 cells were seeded at an appropriate density onto glass coverslips coated with poly-L-lysine (neuVitro) in 24 well plates. The following day each well was transfected with 500 ng of plasmid DNA, 1.75 μL lipofectamine LTX and 0.5 μL PLUS reagent in 100 μL of OPTIMEM I (all ThermoFisher Scientific). For phosphorylation of the TDP-43-WT, TDP-43-C35 and TDP-43-C25 cells were transfected with lipofectamine 2000 (ThermoFisher Scientific), all other transfections of Cos-7 cells used lipofectamine LTX. Again 500 ng of plasmid with 1.75 μL of lipofectamine 2000 were made up in 100 μL of OPTIMEM I and incubated at room temperature for 5 mins. All transfection mixtures were added to each well containing 400 μL of DMEM with high glucose supplemented with 10% FBS and no antibiotics. Transfection mixtures were left on overnight until the time of the experiment. All experiments begun 19-24 hr post-transfection. Cells were exposed to oxidative stress by incubating cells at 37°C with 5% CO_2 in either DMEM supplemented with 10% FBS and antibiotics or DMEM media supplemented with 10% FBS, penicillin-streptomycin and the indicated concentration of sodium arsenite (Sigma-Aldrich). For stress-resolution experiments, cells were exposed to 0.25 mM sodium arsenite for 1 hr and then washed with PBS twice and then incubated in pre-warmed DMEM with 10% FBS and antibiotics. See below for immunofluorescence details.

For drug inhibitor assays, Cos-7 cells were grown on glass coverslips in 24-well plates and transfected with lipofectamine LTX as described above. Transfection mixtures were not removed. Cells were incubated with 1 μM XAV-939 (SelleckChem), G007-LK (SelleckChem) in DMEM with high glucose and 10% FBS for 30 mins at 37°C with 5% CO_2 before the application stress. For IWR1-endo (SelleckChem) experiments, cells were incubated in either 0.5 μM, 1 μM or 10 μM of drug for 30 mins at 37°C with 5% CO_2 prior to stress. For all drugs, cells were exposed to 0.25 mM sodium arsenite in DMEM with high glucose and 10% FBS and the indicated amount of drug for 30 mins at 37°C with 5% CO_2. Experiments commenced 22-23 hr after transfection. See below for immunofluorescence see details.

Primary cortical neurons, in 12-well plates, were cultured in neuralbasal medium with serum-free B-27 (ThermoFisher Scientific) and penicillin-streptomycin (ThermoFisher Scientific). Transfection was carried 6 DIV. Immediately before transfection the culture media was removed and cells were washed twice in pre-warmed PBS with calcium chloride and magnesium chloride (ThermoFisher). 1 ml of pre-warmed neuralbasal medium supplemented with B27 was added to each well. Transfection reactions were made up in a total of 200 μL of OPTIMEM I (ThermoFisher Scientific) and contained 500 ng or 1000 ng (both work well) of plasmid DNA and 2 μL of lipofectamine 2000 (ThermoFisher Scientific). Transfection mixtures were left at room temperature for 5 minutes before being added to the well. The transfection media was removed after 6 hr, each well was washed twice with pre-warmed PBS with calcium chloride and magnesium chloride, and then the cells were returned to pre-warmed and conditioned neuralbasal media supplemented with serum-free B-27 (ThermoFisher Scientific) and penicillin-streptomycin (ThermoFisher Scientific). The neurons were stressed 10 DIV (4 days post-transfection). Transected neurons were stressed in 0.5 mM sodium arsenite for 90 min. See below for immunofluorescence see details.

Neurons and COS-7 cells were fixed for 15 min in 4% paraformaldehyde (made up in 50 mM HEPES pH 7.4, 150 mM NaCl, 1 mM MgCl and 1 mM EGTA), permeablized by 3 sets of 3 mins in PEM-T buffer (100 mM PIPES, 1 mM MgCl2, 10 mM EGTA pH 6.8, and 0.1% Triton X-100), and blocked in 10% normal donkey serum (Sigma-Aldrich) made up in TBST (TBS supplemented with 0.05% TWEEN 20 pH 8). Primary antibodies were applied overnight at 4°C (see below for antibody details) in a humidified chamber, cells were washed 3 times in PEM-T buffer (3 mins each) and secondary antibody was applied for 45 mins (COS-7 cells) or 1 hr (neurons) at room temperature and in the dark. Cells were washed 3 times in TBST (3 mins each), cells were stained with Hoescht for 5 mins and coverslips were washed in deionized H_20 immediately before mounting in prolong diamond.

For detection of PAR, endogenous TDP-43 and Tankyrase in arsenite-induced stress granules, cells were washed twice in dPBS without magnesium and without calcium and extracted in 50 mM HEPES pH 6.8, 150 mM NaCl, 1 mM $MgCl_2$, 1 mM EGTA and 0.1% Triton X-100 for 30 s before fixing. Cells were fixed for 15 mins in 4% paraformaldehyde, permeabilized in PEM-T (3 incubations, 3 mins each), then in 100 mM sodium periodate (Sigma-Aldrich) made up in PEM-T for 5 mins, washed in PEM-T for 3 mins, 25 mM succinic dihydrazide (Sigma-Aldrich) made up in PEM-T (30 mins), 3 washes in PEM-T (3 mins each) and then blocked in 10% normal donkey serum in TBST (TBS supplemented with 0.05 % TWEEN 20 pH 8) for 1 hr at room temperature.

Primary antibodies used for both COS-7 and neurons: mouse anti-TIAR (1 in 500; BD Biosciences), mouse anti-Ataxin-2 (1 in 500; BD Biosciences), rabbit anti-G3BP1 (1 in 1000; Thermo Scientific), goat anti-eIF3 (1 in 50; Santa Cruz Biotechnology), mouse anti-eIF3 (1 in 500; Santa Cruz Biotechnology), rabbit anti-TDP-43 (1 in 300, Proteintech), mouse anti-PAR (1 in 400: Tulip BioLabs), mouse anti PAR (1 in 400, ENZO), mouse pS409/10 (1 in 1000; Cosmo Bio USA) and rabbit pS409/10 (1 in 1000; Cosmo Bio USA). Alexa Fluor −488, −568, −594 and −647 secondary antibodies were used for detection (all 1 in 500; Thermo Scientific).

All experiments were performed at least three independent times.

Image quantification and statistics

All imaging was performed on a Leica DMI6000 unless stated otherwise. To quantify the formation of stress granules in the cytoplasm we captured 4-8 independent images at 20X. The number of cells were quantified by ImageJ software (Rueden et al., 2017) and up to 900 cells per condition per experiment were quantified. The number of cells with 2 or more stress granules were counted. An overall percentage was obtained from three independent experiments and the mean (± SEM) was calculated. To quantify TDP-43-foci formation 4 non-overlapping images at 20X were captured for the WT, C35 and C25 experiments and up to 66 transfected cells were quantified per condition per experiment. These experiments were repeated 3 independent times and a mean (± SEM) was calculated. For the $PBM_{hnRNPA2/B1}$ experiments 6 independent images at 20X were captured and up to 391 transfected cells were quantified. These experiments were repeated 3 independent times and a mean (± SEM) was calculated.

To quantify the recruitment of TDP-43 to stress granules we captured 4-5 independent images at 40X of cells that had both TIAR-labeled stress granules (or one of the other stress granule markers) and cytosolic TDP-43 foci, up to 440 stress granules were quantified per condition per experiment. A mean (± SEM) was calculated from three independent experiments. To quantify the percentage of TDP-43-GFP foci co-labeled with G3BP1 or TIAR, the same images were analyzed and up to 1419 TDP-43-GFP foci were quantified for the presence of TIAR or G3BP1. These experiments were repeated 3 independent times and a mean (± SEM) was calculated.

To quantify the recruitment of TDP-43 to neuronal stress granules we imaged up to 6 transfected neurons and up to 40 stress granules per condition and quantified the number of stress granules localizing with TDP-43. A mean (± SEM) was calculated from three independent experiments.

To quantify the phosphorylation of TDP-43-WT, C35 and C25, 4 non-overlapping images were captured at 20X magnification for each condition, up to 124 transfected cells were quantified per condition per experimental repeat. The percentage of cells with TDP-43 foci and phosphorylated foci was calculated for each condition. For the $PBM_{hnRNPA2/B1}$, experiments 6 non-overlapping images were captured at 20X magnification for each condition, up to 700 transfected cells were quantified. These experiments were repeated 3 independent times and a mean (±s.e.m.) was calculated.

All triple labeled experiments were imaged using a Leica SP5 confocal. TFP-43-YFP and TDP-43-GFP alone were used as a control slide to optimize the settings for fluorescence bleed through. Cells with both G3BP1/TIAR/eIF3-labeled stress granules and cytoplasmic TDP-43-YFP or TDP-43-GFP foci were imaged at 40X magnification, 7-27 transfected cells were quantified per condition per experiment. Experiments were performed 3-5 independent times. Statistics for all experiments were performed using Graphpad prism 6 software.

Statistics (t tests, one-way ANOVA, two-way ANOVA and multiple comparison tests) for all experiments were performed using Graphpad prism 6 software, the details for each experiment are described in each legend.

Fluorescence recovery after photobleaching

COS-7 cells were cultured as described above. For live cell-culture experiments COS-7 cells were grown in a poly-d-lysine coated glass bottom 35 mm culture dish (MatTek). Cells were transfected with using 7 μL lipofectamine LTX, 2 μL of plus reagent (both ThermoFisher Scientific) and 2000 ng of plasmid DNA in a total of 400 μL of OPTIMEM I (all ThermoFisher Scientific) in 1.6 mL DMEM with high glucose and 10% FBS. The transfection reagent was not removed and experiments were performed 21 hr after transfection. FRAP experiments were performed on a laser scanning Leica SP8 confocal with the FRAP module located at the CDB microscopy core, University of Pennsylvania. A cell-culture climate chamber was attached to the microscope stage. The temperature control of the chamber was previously calibrated with thermocouple measurements such that heating the outside of the chamber to 39°C gave an internal temperature of 37°C. An objective heating collar was attached to a 40X water immersion objective and the temperature was set to 33°C. The chamber was attached to a mixed gas chamber. The cell-culture dish was placed in the chamber, the media was removed and rinsed in PBS and then incubated in DMEM with high glucose, 10% FBS and 1x penicillin-streptomycin in the presence or absence of 0.25 mM sodium arsenite.

For FRAP experiments, images collected were 12 bit and at a resolution of 512 by 64. Scanning was unidirectional and at frequency of 1800 Hz with a zoom of 7.5 and a line average of 1. Care was taken to assure that the temperature of the microcopy room did not

increase above 23°C during data acquisition. Conditions for diffuse TDP-43 were; pre-bleaching, 0.2% of the 488 nm laser, for 90 iterations at 76 ms; for bleaching, 100% of the 488 nm laser was used for 360 iterations at 76 ms; and for post-bleach, 0.2% of the 488 nm laser for 2500 iterations at 76 ms was used. Conditions for the TDP-43 foci for pre-bleaching, 0.2% of the 488 nm laser, for 50 iterations at 76ms; for bleaching, 100% of the 488 nm laser for 150 iterations at 76 ms to bleach and 0.2% of the 488 nm laser for 1750 iterations at 76 ms for the post-bleach. One GFP-positive granule was bleached per cell. Bleaching was focused on a circular region of interest (ROI) set to 1 micron in diameter. For early stress, cells were bleached from 30 mins to 1 hr and for late stress cells were bleached after 2 hr of treatment. 7 to 14 cells were bleached for each condition. Each experiment was more than performed 3 independent times and on different days. After image capture, an ROI was applied to a non-bleached GFP-positive granule (to account for photobleaching). The intensity data of the ROIs were normalized and exported as a csv file.

To determine the rate of fluorescence recovery (FR) the fluorescence of the bleached ROI was normalized to the unbleached ROI at every time point (t) to take into account changes in fluorescence during image acquisition:

$$\left(Ft_{(bleached)} / Ft_{(unbleached)}\right)$$

These data were then used to calculate the rate of fluorescence recovery (FR) for each time point (t) with the following formula:

$$FRt = \left(Ft_{(bleached)} - Ft_{(Initial\ bleach)}\right) \cdot \left(Ft_{(Prebleach)} - Ft_{(Initial\ bleach)}\right)$$

Each condition was repeated three times each on different days. The data from each experiment was plotted in Graphpad Prism 6 and a one-phase decay curve was extrapolated from the data with 1000 iterations per time point. From the curve the half time ($t_{1/2}$) and the plateau (mobile/immobile fraction) was calculated. A Fisher's test was performed to identify significant differences.

GST-TDP-43 protein purification

N-terminally tagged GST-TDP-43-WT was overexpressed in BL21(DE3)RIL *E. coli*. The *E.coli* cells were then lysed by sonication on ice in 40 mM HEPES (pH 7.4), 5 mM EDTA, 300 mM KCl, 1 mM DTT, 5% glycerol, 5 μM pepstatin, 10mg/l RNase A and protease inhibitors (cOmplete, EDTA-free, Roche Applied Science). The protein was purified over Glutathione Sepharose 4 Fast Flow beads (GE Healthcare) and eluted from the beads using 40 mM HEPES (pH 7.4), 150 mM NaCl, 5% glycerol, and 20 mM reduced glutathione.

PAR polymer

Free PAR polymer (commercially obtained from TREVIGEN) was synthesized from PARP-1 and ranged in size from 2-300 ADP-ribose subunits. Molar equivalencies were calculated by TREVIGEN, briefly, the Absorbance of the PAR at 258 nm was divided by the extinction coefficient of ADP-ribose (13, 500 cm^{-1} M^{-1}) (Schultheisz et al., 2009; Shah et al., 1995).

PAR-binding dot blot assay

PAR-binding motifs were identified by aligning the PBM consensus to TDP-43 using the PATTINPROT search engine (Combet et al., 2000). For dot-blot analysis of recombinant protein, 0.25-0.5 μg of protein, diluted in 40 mM hepes (pH 7.4), 150 mM NaCl, 5% glycerol and 20 mM reduced glutathione, was blotted onto 0.45 micron nitrocellulose membrane. Peptides, synthesized by GenScript (details are in the Key Resources Table and Figure 2), were spotted onto 0.1 micron nitrocellulose at 0.25-0.5 μg. Membranes were left to dry for 60-90 mins and then incubated in dPBS supplemented with 0.05% TWEEN20 (PBST) for 30 mins without agitation. The membrane was sealed in a hybridization bag (KPL) containing 0.4 mL of PBST containing 50nM PAR polymer (Trevigen) and incubated for 1 hr with rocking and rotation at room temperature. The membrane was washed 5 times in PBST (5 mins each) and blocked in PBSMT (5% milk in PBST) for 1 hr then incubated in primary antibody in PBST for 1 hr. After 5 washes in PBSMT (5 min each), the membrane was incubated with secondary antibody in PBSMT for 30 min. The membrane was washed 3 times in PBSMT, 2 times in PBST and 2 times in PBS (all 5 min each). ECL prime was used to detect secondary antibody. Antibodies used were anti-PAR (10H) (1 in 250; Tulip Biolabs and 1 in 500; ENZO) anti-TDP-43 (1 in 3000; Proteintech). HRP-coupled secondary antibodies used: goat antibody to rabbit (1 in 5,000; EMD Millipore) and goat antibody to mouse (1 in 2,000; Jackson ImmunoResearch Laboratories, Inc. and 1 in 5000; abcam). For SYPRO Ruby staining, blotted and dried membranes were submerged in PBS and then incubated in 7% acetic acid and 10% methanol for 15 minutes, the membrane was washed 4 times (5 mins each) in deionized H_2O with gentle rotation, the membrane was incubated in SYPRO Ruby blot stain (ThermoFisher Scientific) for 30 min in the dark, washed 4 times in deionized H_2O (5 mins each) and imaged on a Safe Imager (ThermoFisher Scientific). The dot blot was carried out 6 independent times and in addition was repeated on independent preparation of proteins. Spot intensities were measured using ImageJ software (Rueden et al., 2017) and statistics were performed using Graphpad prism 6 software.

Purification of Recombinant His_6-SUMO-TDP-43

His_6-SUMO N-terminally tagged TDP-43-WT was overexpressed in BL21(DE3)RIL *E. coli*. The *E.coli* cells were then lysed by sonication on ice in 50 mM HEPES (pH 7.5), 2% Triton X-100, 500 mM NaCl, 30 mM imidazole, 5% glycerol, 2 mM β-mercaptoethanol, and protease inhibitors (cOmplete, EDTA-free, Roche). The protein was purified over Ni-NTA agarose beads (QIAGEN) and eluted from the beads using 50 mM HEPES (pH 7.5), 500 mM NaCl, 300 mM imidazole, 5% glycerol, and 5 mM DTT. The protein was

subsequently buffer exchanged into 50 mM HEPES (pH 7.5), 500 mM NaCl, 5% glycerol, and 5 mM DTT, flash frozen in liquid N_2, and stored as aliquots in −80°C until use. His_6-SUMO N-terminally tagged TDP-43-ΔPBM and TDP-43-Q331K were purified using the protocol described above. Note: for C35 and C25, the expression was induced with 1 mM IPTG for 2 hours at 37°C whereas for all the other proteins it was with 1 mM IPTG for 16 hours at 15°C.

Purified His_6SUMO-TDP-43 was thawed and centrifuged at 16,100 X *g* for 10 min at 4°C to remove preformed aggregates. Protein concentration was determined by Bradford assay (Bio-Rad). The purity of the expressed proteins was confirmed on a 4%–20% polyacrylamide gel.

Purification of Recombinant TDP-43-MBP-His_6

The plasmid encoding TDP-43-MBP-His_6 was purchased from addgene (plasmid #104480) and expressed in BL21 (DE3) RIL *E. coli*. following the conditions reported previously (Wang et al., 2018). Cells were harvested by centrifugation, resuspended in TDP-43 binding buffer (20 mM Tris–Cl pH 8.0, 1 M NaCl, 10 mM imidazole, 10% (v/v) glycerol, 1 mM DTT) supplemented with cOmplete EDTA-free protease inhibitor cocktail, and lysed using an Emulciflex C-3. The protein was purified over Ni-NTA agarose beads (QIAGEN) and eluted from the beads using 20 mM Tris–Cl pH 8.0, 1 M NaCl, 300 mM imidazole, 10% (v/v) glycerol, 1 mM DTT. The eluate was further purified over amylose resin (NEB) and eluted from the amylose resin using 20 mM Tris–Cl pH 8.0, 1 M NaCl, 10mM maltose, 10% (v/v) glycerol, 1 mM DTT. The protein was concentrated, flash frozen in liquid N_2, and stored as aliquots in −80°C until use.

Liquid-droplet formation

His_6-SUMO-TDP-43 was prepared in 50 mM HEPES-NaOH (pH 7.5), 5% (v/v) glycerol, 5 mM DTT, and 100 mg/mL dextran from *Leuconostoc spp.* (Sigma, St. Louis, MO) with the indicated concentrations of NaCl. For TDP-43-MBP-His_6, the protein was first buffer exchanged into 20 mM HEPES, pH 7.4, 150 mM NaCl, 1 mM DTT and reactions were prepared in 20 mM HEPES, pH7.4, 1 mM DTT, 100 mg/mL dextran from *Leuconostoc spp.* (Sigma, St. Louis, MO) with the appropriate concentration of NaCl. Protein was always added last to each LLPS reaction. Protein samples were spotted onto a coverslip and imaged by differential interference contrast (DIC) microscopy. All movies and images were captured within ten minutes of reaction set-up. Details of experimental repeats are in the associated legends.

To assess the effect of PAR on TDP-43 phase separation, SUMO-TDP-43 was prepared as before but with the addition of 5 microM mono-ADP- ribose equivalents of PAR (Trevigen) or equivalent volume of PAR control buffer (10 mM Tris, pH8 and 1mM EDTA). For SUMO-TDP-43 and PAR experiments, all movies and images were captured within ten min of reaction set up. For TDP-43-MBP-His_6 with PAR or PAR control buffer, reactions were incubated at room temperature (~19 −22°C) for 1 hr prior to imaging.

The PAR nucleation studies of TDP-43 LLPS were repeated twice at the phase boundary. The comparison between full-length TDP-43 and TDP-43 with mutation in the PAR-binding motifs has been tested three times on two or more different protein preps. The comparison between full-length TDP-43 and the C-terminal fragments has been repeated on two independent protein preps. Testing the effect of PAR on the TDP-43-WT, TDP-43-ΔPBM and the two C-terminal fragments has been repeated on two independent protein preps. Experiments examining the phase boundary of TDP-43-MBP were performed 3-5 times and experiments analyzing PAR nucleation three times using one protein prep. Further details are in each associated legend.

QUANTIFICATION AND STATISTICAL ANALYSIS

All data points in each graph are mean (± SEM) and the n is a biological repeat. T Tests, one-way ANOVA, two-way ANOVA and multiple comparison tests were performed, and are described in each figure legend. Significance was set at $p < 0.05$. All statistical analyses were carried out using Graphpad prism6 software.

DATA AND SOFTWARE AVAILIBILITY

Raw datasets are available in Mendeley Data and are available at https://data.mendeley.com/datasets/rh7zv7w8c8/1.

Molecular Cell, Volume *71*

Supplemental Information

Poly(ADP-Ribose) Prevents Pathological Phase Separation of TDP-43 by Promoting Liquid Demixing and Stress Granule Localization

Leeanne McGurk, Edward Gomes, Lin Guo, Jelena Mojsilovic-Petrovic, Van Tran, Robert G. Kalb, James Shorter, and Nancy M. Bonini

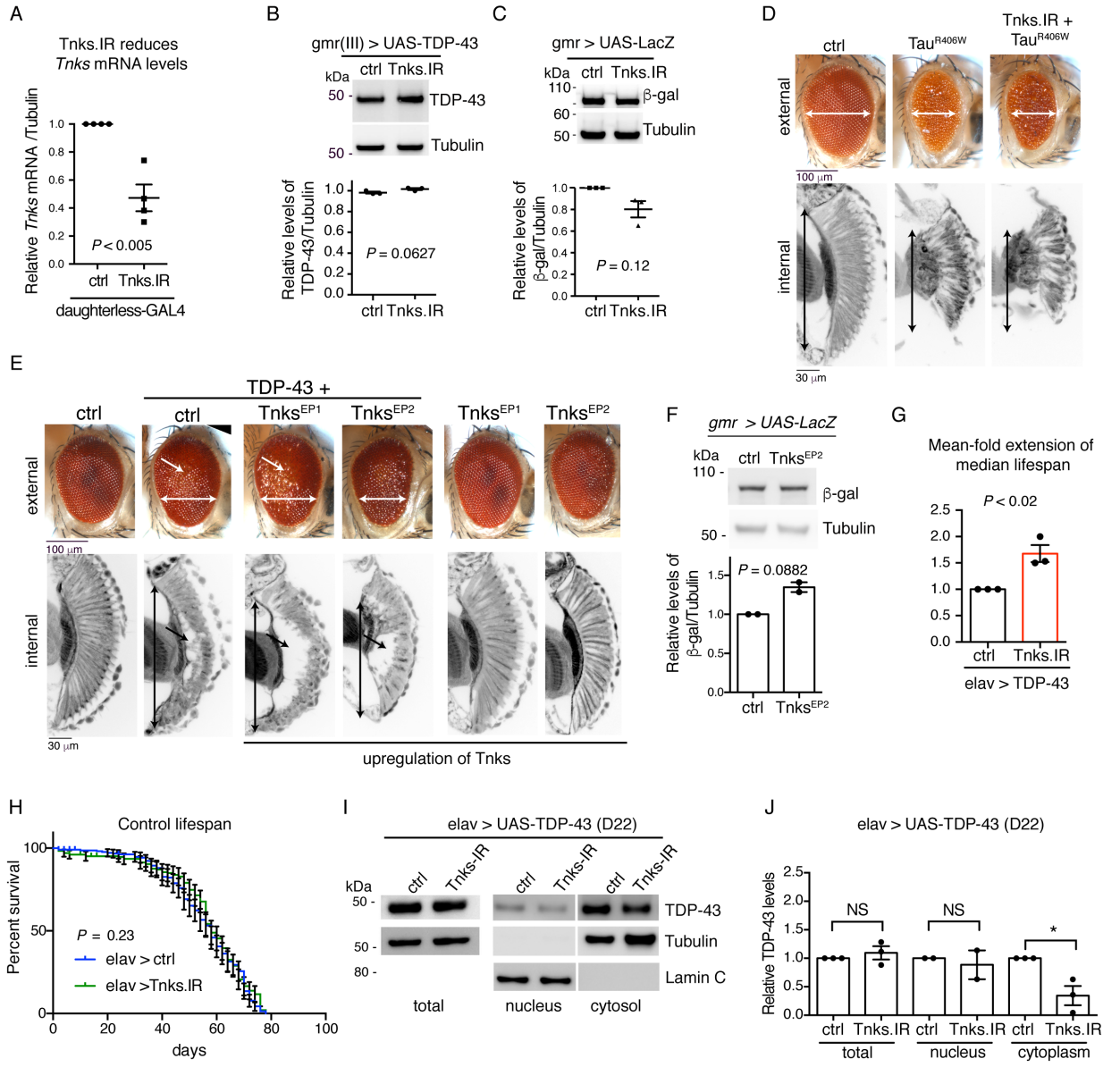

Supplementary Figure 1 (Related to Figure 1): Tankyrase is a genetic modifier of TDP-43.

(A) Expression of the *UAS-tankyrase* RNAi transgene (Tnks.IR) in fly larvae with the *daughterless-GAL4* (*da-GAL4*) driver leads to a significant reduction in *tankyrase* (*Tnks*) mRNA compared to control (ctrl). The graph represents the mean (± SEM) of 4 independent experiments. An unpaired and two-tailed T test was used to determine significance ($p < 0.005$). Control (ctrl) genotype is *da-GAL4/+* and the Tnks.IR genotype is *da-GAL4/UAS-Tnks-IR$^{4179R-4}$; +/+*.

(B) Reduction of *Tnks* (Tnks.IR) had no effect on TDP-43 protein levels. The Tnks.IR transgene was co-expressed with TDP-43 in the fly eye with the *gmr-GAL4* driver and total protein extract was isolated from heads of day-1-old female flies. The mean (± SEM) of TDP-43 protein levels relative

to Tubulin was calculated from three independent experiments. An unpaired and two-tailed T test revealed that no significant difference was detected in the total levels of TDP-43 between the experimental and control (ctrl) genotype. The ctrl genotype is *UAS-TDP-43 (37M)/+; gmr-GAL4 (III)/+* and the Tnks.IR genotype is *UAS-TDP-43 (37M)/ UAS-Tnks-IR$^{4179R-4}$*; *+/+*.

(C) Reduction of *Tnks* (Tnks.IR) had no effect on the GAL4-binary system. The Tnks.IR transgene and the *UAS-LacZ* reporter transgene were co-expressed in the fly eye with the *gmr-GAL4* driver. Total protein was isolated from the heads of female flies at day 1 and the levels of the *lacZ* protein, β-galactosidase (β-gal), and Tubulin were measured by immunoblot. The graph represents the mean (± SEM) of three independent experiments. An unpaired T test was performed to reveal that β-gal levels were not statistically different between the control (ctrl) and experimental genotype. The ctrl genotype is *gmr-GAL4 (II*), *UAS-LacZ*/*UAS-mCD8-GFP*; +/+ and the experimental Tnks-IR genotype: *gmr-GAL4 (II), UAS-LacZ / UAS-Tnks-IR$^{4179R-4}$; +/+*.

(D) Reduction of *Tnks* has no effect on the toxicity of the Alzheimer's and frontotemporal degeneration-associated protein Tau. White arrowheads indicate width of external retina and black arrowheads indicate the length of the internal retina. The control (ctrl) genotype is *gmr-GAL4/UAS-mCD8-GFP; +/+*, the Tau R406W genotype is *gmr-GAL4/UAS-mCD8-GFP; UAS-Tau R406W/+*, and the Tau R406RW + Tnks.IR genotype is *gmr-GAL4/ Tnks-IR$^{4179R-4}$; UAS-Tau R406W/+*.

(E) Upregulation of *Tnks* enhances TDP-43-associated toxicity in the fly eye, while upregulation of *Tnks* alone in the fly eye has no effect on the external (upper panel) or internal retina (lower panel). White arrowheads indicate width of external retina, white arrows point to roughening of the external eye, black arrowheads indicate the length of the internal retina and black arrows indicate vacuolization of the internal retina. Control genotype is *UAS-mCD8-GFP/+*; *gmr-GAL4* (III*)/+.* TDP-43 + ctrl is *UAS-TDP-43(M)*/*UAS-mCD8-GFP*; *gmr-GAL4* (*III*)*/+. TDP-43 + Tnks^{EP1}* is *UAS-TDP-43(M)*/+; *gmr-GAL4* (*III*)/*Tnks [EPg]Tnks^{HP37069}*. TDP-43 + Tnks^{EP2} is *UAS-TDP-43(M)*/+; *gmr-GAL4* (*III*)/*Tnks [EP]Tnks^{EP3476}*. Tnks^{EP1} *is +/+; gmr-GAL4* (*III*)/*Tnks [EPg]Tnks^{HP37069}* and Tnks^{EP2} is +/+; *gmr-GAL4* (*III*)/*Tnks [EP]Tnks^{EP3476}*.

(F) Upregulation of *Tnks* in the eye with *gmr-GAL4* had no effect on the GAL4 system. Total protein was isolated from the heads of female flies at day 1 and the levels of the *lacZ* protein, β-galactosidase (β-gal), and Tubulin were measured by immunoblot. The graph represents the mean (± SEM) of two independent experiments. A one-way ANOVA was performed to reveal that β-gal levels were not statistically different between the control (ctrl) and experimental genotype. Ctrl genotypes is *gmr-GAL4 (II*), *UAS-LacZ*/*UAS-mCD8-GFP*; *+/+*. Tnks^{EP2} is *gmr-GAL4 (II*), *UAS-LacZ*/+; +/ *Tnks [EP]Tnks^{EP3476}*.

(G) Reduction of *Tnks* (Tnks.IR) in the nervous system of the fly extends the median lifespan of TDP-43 flies. Data represent the mean-fold extension of the median lifespan (± SEM) of elav > TDP-43 compared to elav > TDP-43+Tnks.IR, n=3 independent lifespan assays. An unpaired T test with equal variance was performed. More than 150 male flies were followed per genotype, and

this was performed three independent times. The elav > TDP-43 + ctrl genotype is *UAS-mCD8-GFP/+*; *elav3A-GAL4, UAS-TDP-43 (S)/ +*. elav > TDP-43+Tnks.IR is *UAS-Tnks-IR*$^{4179R-4}$/+; *elav3A-GAL4, UAS-TDP-43 (S)*/+.

(H) Reduction of *Tnks* (Tnks.IR) in the nervous system in the fly has no effect on the lifespan of the fly compared to the elav control. More than 214 male flies were followed throughout the experiment per genotype. A log-rank test for trend ($p > 0.2$) was performed. Genotypes: elav > control (ctrl) is *UAS-mCD8-GFP/+*; *elav3A-GAL4/+* and elav >Tnks.IR is *UAS-Tnks.IR/+; elav3A-GAL4/+*.

(I) Reduction of *Tnks* (Tnks.IR) in the nervous system of the fly has no effect on the total TDP-43 protein levels (aged to 22 days). Reduction of *Tnks* (Tnks.IR) significantly decreases cytoplasmic TDP-43 protein levels. Control (ctrl) genotype is *UAS-mCD8-GFP/+*; *elav3A-GAL4, UAS-TDP-43 (S)/+*. elav > TDP-43 + Tnks.IR genotype is *UAS-Tnks-IR*$^{4179R-4}$/+; *elav3A-GAL4, UAS-TDP-43 (S)*/+.

(J) TDP-43 protein levels were quantified from total protein, nuclear extract and cytosolic extract. The mean (± SEM) of TDP-43 levels relative to Tubulin/LaminC from three independent experiments is presented. A one-way ANOVA ($p = 0.0088$) followed by a Tukey's test was performed to reveal significance (asterisk: $p < 0.05$), NS: not significant.

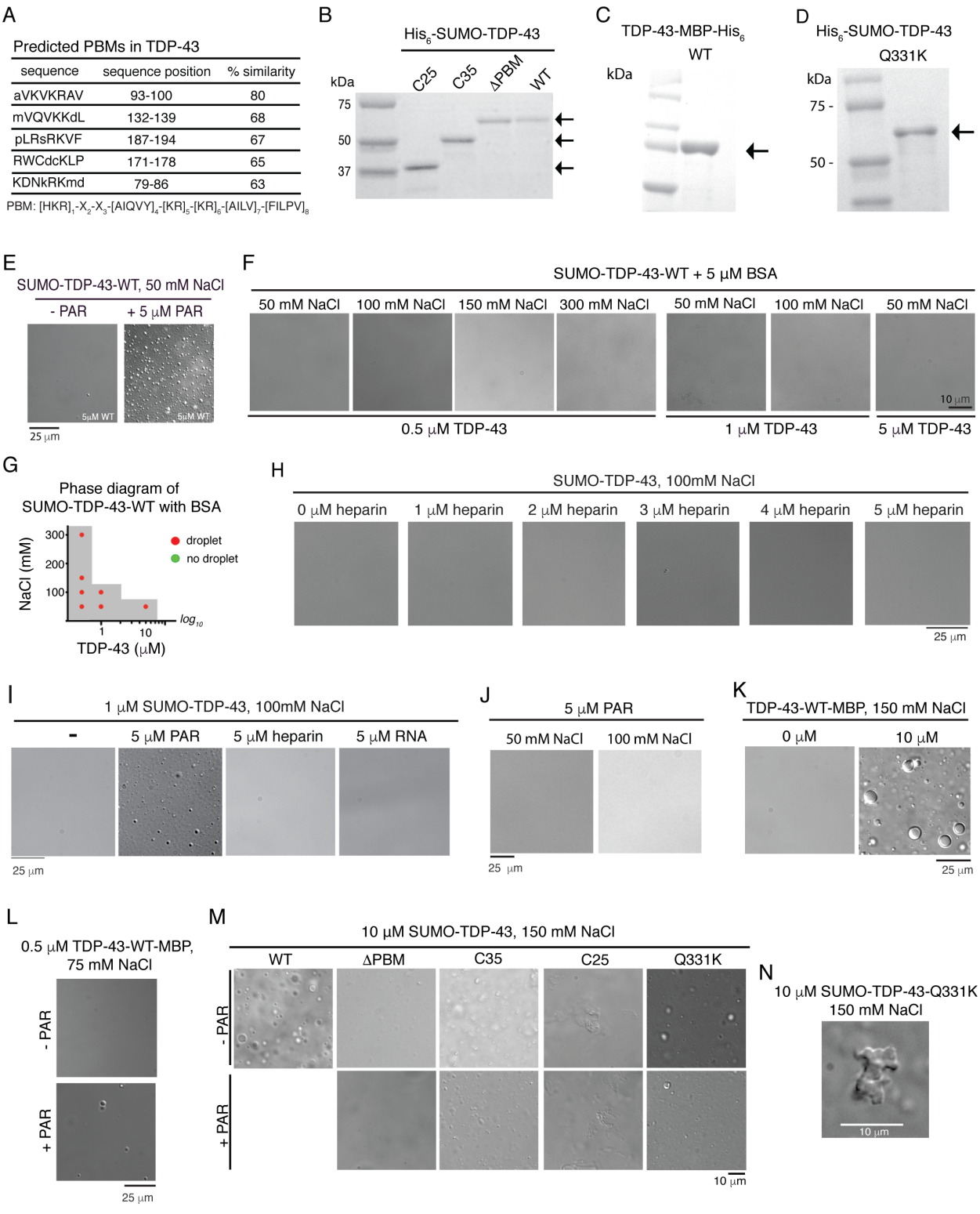

Figure S2 (Related to Figures 2, 3 and 4): PAR nucleates LLPS of TDP-43.

(A) The PAR-binding motif (PBM) consensus was aligned to TDP-43 using the PATTINPROT search engine (Combet et al., 2000). Table lists all regions (and sequence similarity to the PBM) identified in TDP-43.

(B) Expression and purification of HIS_6-SUMO-TDP-43-WT, -ΔPBM, -C35 and -C25 led to pure protein of the correct size (arrows).

(C) Expression and purification of TDP-43-WT-MBP-His_6 led to pure protein of the correct size (arrow).

(D) Expression and purification of HIS_6-SUMO-TDP-43-Q331K led to pure protein of the correct size (arrow).

(E) 5 μM ADP-ribose equivalents of PAR nucleated LLPS of 5 μM SUMO-TDP-43-WT in 50 mM NaCl. This was repeated twice from one preparation of protein.

(F) 5 μM of BSA did not nucleate SUMO-TDP-43-WT LLPS. This was performed on one preparation of protein.

(G) BSA did not nucleate SUMO-TDP-43-WT. Protein and salt concentration pairs are plotted for the presence (green) or absence (red) of protein droplets.

(H) Addition of increasing amounts of heparin (1-5 μM ADP-ribose equivalents) did not promote SUMO-TDP-43-WT LLPS. This was performed on one preparation of protein.

(I) The addition of PAR, stimulated LLPS of 5 μM SUMO-TDP-43-WT in 100 mM NaCl whereas the addition of heparin, yeast total RNA or mono(ADP-ribose) (MAR) at 5 μM ADP-ribose equivalents did not promote SUMO-TDP-43-WT LLPS.

(J) PAR did not undergo LLPS. 5 μM ADP-ribose equivalents of PAR was incubated in 50 mM or 100 mM NaCl. This was performed on one sample of PAR.

(K) 10 μM TDP-43-MBP in 150 mM NaCl underwent LLPS.

(L) 5 μM ADP-ribose equivalents of PAR nucleated LLPS of 0.5 μM TDP-43-WT-MBP in 75 mM NaCl.

(M) Addition of 5 μM ADP-ribose equivalents of PAR did not nucleate LLPS of 10 μM SUMO-TDP-43-ΔPBM, SUMO-TDP-43-C35, SUMO-TDP-43-C25 or SUMO-TDP-43-Q331K in 150 mM NaCl. This was repeated twice from one protein prep.

(N) Example of solid structure formed by TDP-43-Q331K. At lower NaCl concentrations (150 mM, 100 mM and 50 mM) TDP-43-Q331K formed the occasional solid aggregate.

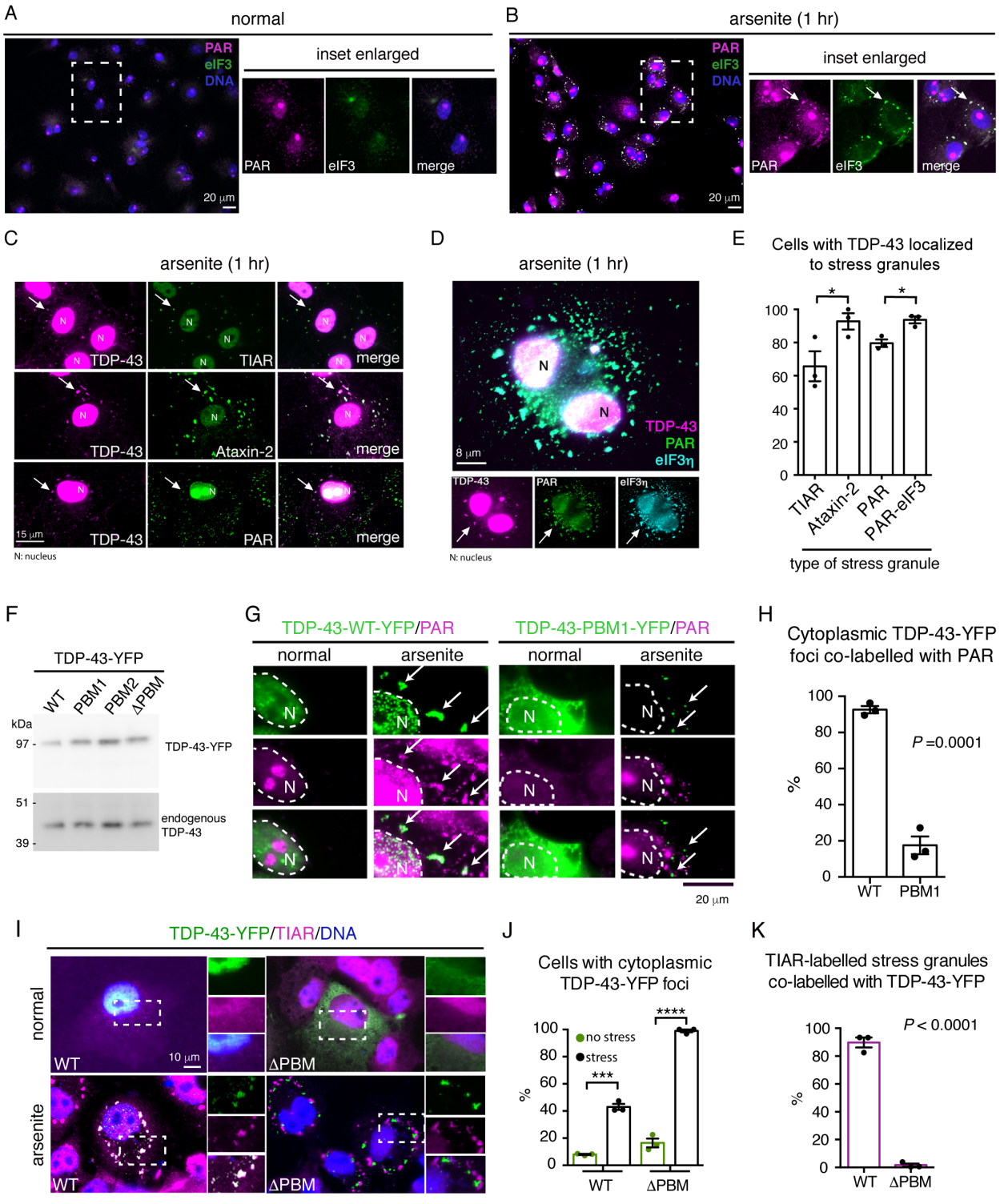

Figure S3 (Related to Figure 5): TDP-43 localization to PAR-containing stress granules is dependent on functional PBMs embedded in the nuclear localization sequence.

(A-B) Stress induces the formation of PAR-containing stress granules (insets and arrows). Cells were immunostained for eiF3η and PAR (Tulip, 10H) and counterstained with Hoescht. 100% of eIF3-positIve stress granules contained PAR. 5 images at 40X magnification and ~25-100 cells and 400 or more eIF3η-positive stress granules were quantified. This experiment was repeated three independent times. Arrows indicate cytoplasmic PAR foci. Scale bar: 30 μm.

(C) After treatment with 0.5 mM sodium arsenite (1 hr), endogenous TDP-43 localized to stress granules that were immunoreactive for TIAR, Ataxin-2, and PAR. Arrows indicate cytoplasmic TDP-43 foci. Scale bar: 15 μm.

(D) Upon treatment with 0.5mM sodium arsenite (1 hr) endogenous TDP-43 localized to stress granules immunolabelled with both PAR (Tulip, 10H) and eIF3η. Arrows indicate cytoplasmic TDP-43 foci. Scale bar: 8 μm.

(E) The percentage of cells with arsenite-induced stress granules labelled with TIAR, Ataxin-2, PAR or PAR-eIF3η were quantified for colocalization with endogenous TDP-43. Five images at 40X magnification, per condition, were quantified. The graph represents the mean (± SEM) of three independent experiments. One-way ANOVA ($p < 0.05$) and a Tukey's test was performed. Asterisks: significant pairs.

(F) Expression of TDP-43-WT-YFP and TDP-43-ΔPBM-YFP in mammalian cells leads to the production of full-length protein at comparable levels. Blots were immunoblotted for TDP-43, and endogenous TDP-43 is presented as the internal control. Note TDP-43-PBM2-YFP was not presented in this study but was included in the figure so that the gel was uninterrupted.

(G) Stress induces the formation of cytoplasmic foci of TDP-43-WT-YFP that co-label for PAR. Stress induced the formation of TDP-43-PBM1-YFP foci in the cytoplasm that do not co-label for PAR. Arrows indicate cytoplasmic TDP-43-YFP foci.

(H) The cytoplasmic and stress-induced foci of TDP-43-YFP were quantified for colocalization with PAR. Mutation in the PBM led to a significant reduction in the amount of TDP43-YFP foci that colocalized with PAR.

(I) In mammalian cells, stress-induced foci of TDP-43-WT-YFP localize to TIAR-labelled stress granules whereas stress-induced foci of TDP-43-ΔPBM-YFP are excluded from TIAR-labelled stress granules. Cells were exposed to 0.5 mM sodium arsenite for 1 hr, immunolabelled for TIAR and counterstained with Hoescht.

(J) Cells were quantified for the presence of cytoplasmic foci of TDP-43-YFP. The mean (± SEM) was calculated from three independent experimental repeats. Two-way ANOVA ($p < 0.0001$) and a Tukey's test was performed. Asterisks: significant pairs and NS: not significant.

(K) Cells were quantified for the localization of TDP-43 to TIAR-labelled stress granules. The mean (± SEM) from three independent experiments is presented. An unpaired and two-tailed T Test was performed ($p < 0.0001$).

Asterisks:
***: $p < 0.001$ and ****: $p < 0.0001$.

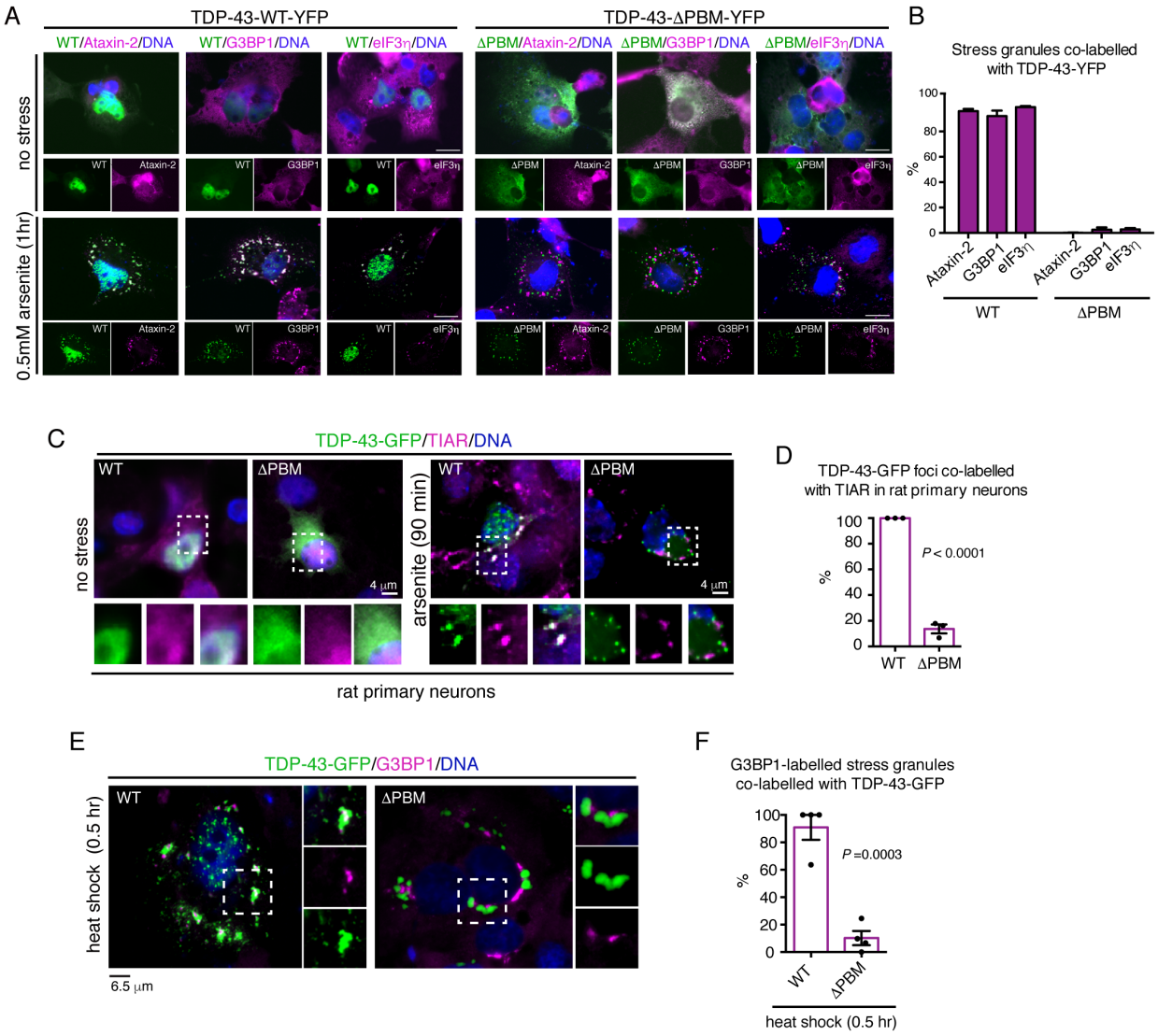

Figure S4 (Related to Figure 5): Mutation of the PAR-binding motifs prevents the recruitment of TDP-43 into stress granules.

(A) Upon treatment with 0.5 mM sodium arsenite (1 hr), TDP-43-WT-YFP and TDP-43-ΔPBM-YFP formed cytoplasmic foci. TDP-43-WT was localized to stress granules whereas TDP-43-ΔPBM formed foci that were excluded from stress granules. Cells were immunostained with antibodies directed to Ataxin-2, G3BP1 and eIF3η. Cells were counterstained with Hoescht. Scale bars: 20 μm.

(B) Cells with both foci of TDP-43 and stress granules were quantified for colocalization. One coverslip was examined per condition. At least 300 stress granules from 5 non-overlapping images at 40X magnification were quantified from each condition. Graph represents the mean (± SEM) of 5 images per condition.

(C) In rat cortical neurons, TDP-43-WT-GFP is nuclear, whereas TDP-43-ΔPBM-GFP is cytoplasmic. In rat cortical neurons, stress-induced foci of TDP-43-WT-GFP localized to TIAR-labelled stress granules, whereas stress-induced foci of TDP-43-ΔPBM-GFP were excluded from TIAR-labelled stress granules. Neurons were exposed to 0.5 mM sodium arsenite for 90 min, immunolabelled with TIAR and counterstained with Hoescht.

(D) Rat cortical neurons with both TIAR-labelled stress granules and cytoplasmic foci of TDP-43 were quantified for colocalization. The mean (± SEM) calculated from three independent experiments is presented. An unpaired and two-tailed T test was performed ($p < 0.0001$).

(E) Upon treatment with heat shock (43^{o}C for 30 min) TDP-43-WT-GFP localized to stress granules whereas TDP-43-ΔPBM-GFP formed foci that were largely excluded from stress granules. Cells were immunostained with an antibody directed to G3BP1 and counterstained with Hoescht.

(F) G3BP1-labelled stress granules were quantified for co-labelling with TDP-43-GFP. A mean (± SEM) from four independent experiments is presented. An unpaired and two tailed T-test was used to test for significance.

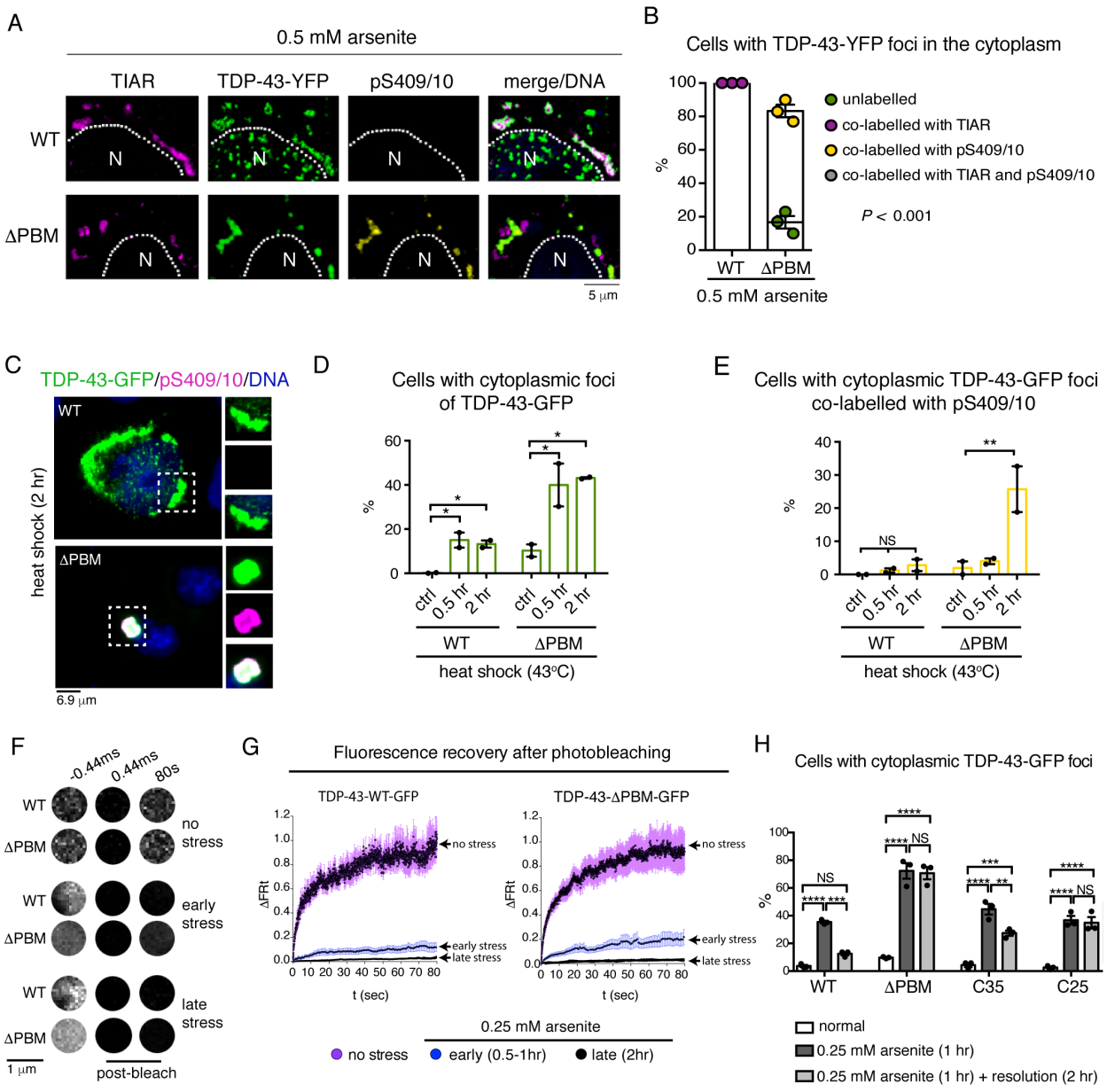

Figure S5 (Related to Figure 6): Exclusion from stress granules leads to phosphorylation of TDP-43 foci that fail to resolve after the removal of stress.

(A) Stress-induced foci of TDP43-WT-YFP recruited to TIAR-labelled stress granules were not co-labelled with pS409/10. Stress-induced foci of TDP-43-ΔPBM-YFP excluded from TIAR-labelled stress granules were co-labelled with pS409/10. Cells were immunolabelled with TIAR and pS409/10, counterstained with Hoescht and imaged by confocal microscopy. N: nucleus and hatched line is the nuclear/cytoplasm boundary.

(B) Cells were quantified for the presence of cytoplasmic TDP-43-YFP foci that were unlabeled, labelled with TIAR, pS409/10 or both TIAR and pS409/10. The mean (± SEM) of three independent experiments is presented. Two-way ANOVA ($p < 0.0001$) was performed.

(C) Heat shock (43^{o}C) induced the phosphorylation of TDP-43-ΔPBM-GFP foci and not TDP-43-WT-GFP foci. Cells were immunostained with an antibody directed to pS409/10 and counterstained with Hoescht.

(D) Cells with cytoplasmic TDP-43-GFP foci were quantified. The graph represents the mean (± SEM) of two independent experiments. A one-way ANOVA ($p < 0.05$) and a Fishers LSD test was used to test for significance. Asterisks: significant pairs.

(E) Cells with cytoplasmic TDP-43-GFP foci co-labelled with pS409/10 were quantified. The graph represents the mean (± SEM) of two independent experiments. A one-way ANOVA ($p < 0.05$) and a Fishers LSD test was used to test for significance. Asterisks: significant pairs. NS: not significant.

(F) The mobility of TDP-43-WT-GFP and TDP-43-ΔPBM-GFP was assessed by fluorescence recovery after photobleaching (FRAP) in live cells. Under normal conditions the mobility of diffuse cytoplasmic TDP-43 was assessed. Under stress the mobility of TDP-43 in cytoplasmic foci was measured during the early stage of treatment with 0.25 mM sodium arsenite (30 min to 1 hr), and during the late stage of stress (2 hr onwards). Shown are the 1 μm regions of interest (ROIs) that were bleached.

(G) The rate of fluorescence recovery after photobleaching was calculated for each condition. The graph (± SEM) represents one experiment for each condition (see arrows in graph). For the normal conditions, more than 7 ROIs, each from a different cell, are plotted. For the early stress more than 12 ROIs, each from an individual foci and cell, is plotted, and for the late stress, more than 6 ROIs, each from an individual foci and cell, are plotted. These experiments were repeated more than three independent times and each time the fluorescence recovery was similar.

(H) Cells were exposed to 0.25 mM sodium arsenite (1 hr), the cells were then left to recover for 2 hr. Cells were quantified for the presence of TDP-43-GFP foci from normal conditions, stress conditions and after resolution. Stress-induced TDP-43-WT-GFP cytoplasmic foci resolved 2 hr after the removal of stress. However, stress-induced foci of TDP-43-ΔPBM-GFP, TDP-43-C35-GFP and TDP-43-C25-GFP did not resolve after 2 hr of recovery. Transfected cells in 5 non-overlapping images (20X magnification) were quantified for the presence of TDP-43-GFP cytoplasmic foci. Graph represents the mean (± SEM) of three independent experiments. Two-way ANOVA ($p < 0.0001$) and a Tukey's test identified significance (asterisks). NS: not significant

Asterisks:
*: $p < 0.05$, **: $p < 0.01$, ***: $p < 0.001$, and ****: $p < 0.0001$.

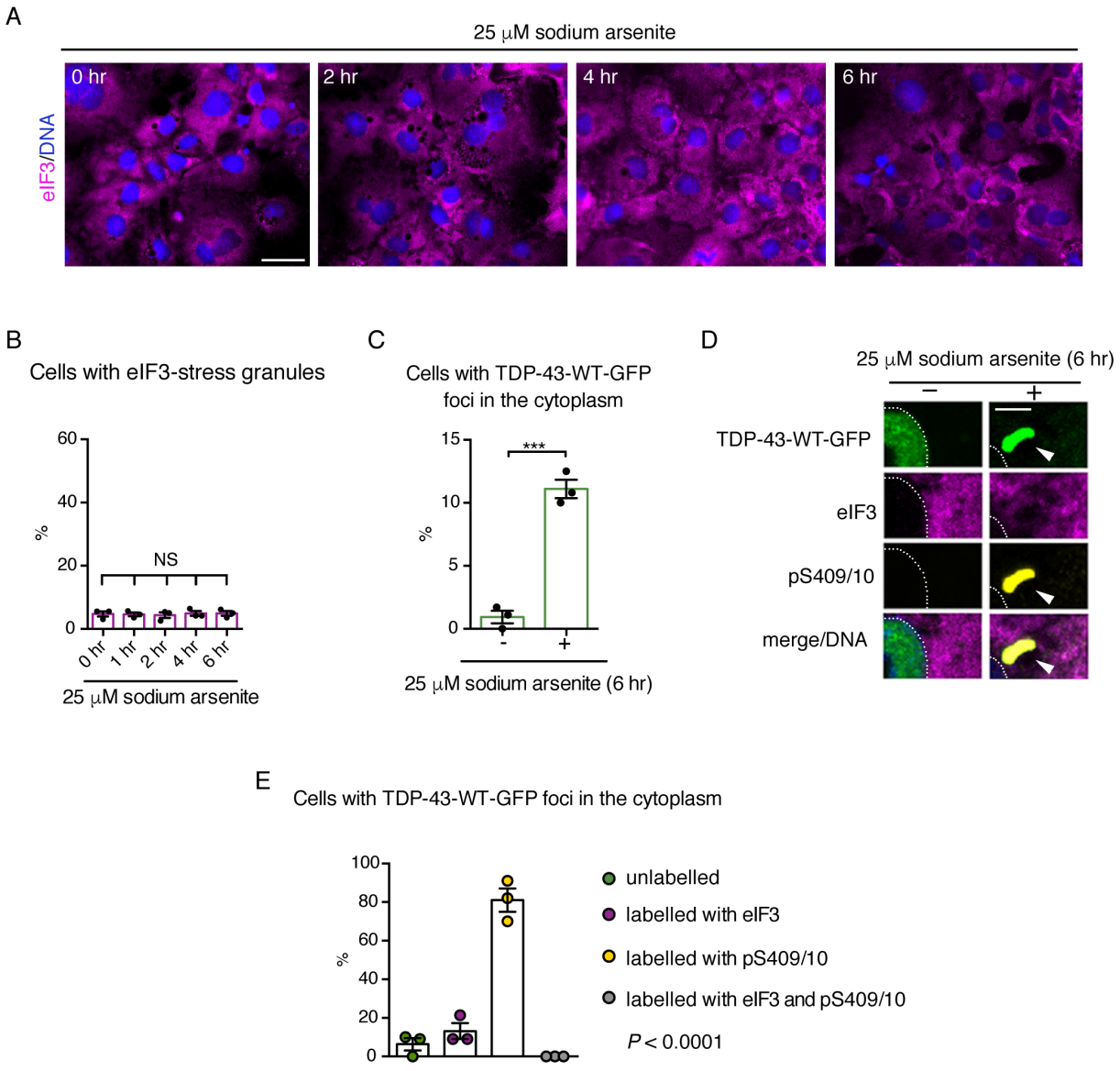

Figure S6 (Related to Figure 7): TDP-43 foci that form under low levels of prolonged stress are phosphorylated.

(A) Treatment with 25 μM sodium arsenite for 6 hr did not lead to the formation of eIF3-labelled stress granules. Cells were immunolabelled for eIF3 and counterstained for Hoescht. Scale bar: 35 μm.

(B) Cells were quantified for the presence of eIF3-labelled stress granules. Four non-overlapping images taken at 20X magnification were quantified from each condition. Graph represents the mean (± SEM) of three independent experiments. NS: not significant.

(C) Cells were quantified for cytoplasmic TDP-43-WT foci. The mean (± SEM) of three independent experiments is presented. See methods for details. One-way ANOVA ($p = 0.0003$) was performed.

(D) Exposure to 25 μM sodium arsenite for 6 hr resulted in cytoplasmic TDP-43-WT foci that lacked eIF3 and were co-labelled for pS409/10 (arrowheads indicate TDP-43-WT foci that are labelled with pS409/10). Cells were labelled for eIF3, pS409/10 and Hoescht, and imaged by confocal microscopy. Scale bar: 3.5 μm.

(E) Cells with cytoplasmic TDP-43-WT foci were quantified as unlabeled, labelled with eIF3, pS409/10 or both. After 6 hr of treatment with 25 μM sodium arsenite there was an increase in the percentage of cells with phosphorylated (pS409/10) TDP-43-WT foci and a decrease in the percentage of cells with TDP-43-WT foci co-labelled with eIF3. One-way ANOVA ($p < 0.0001$) and a Tukey's test was performed.

Asterisks:

***: $p < 0.001$.

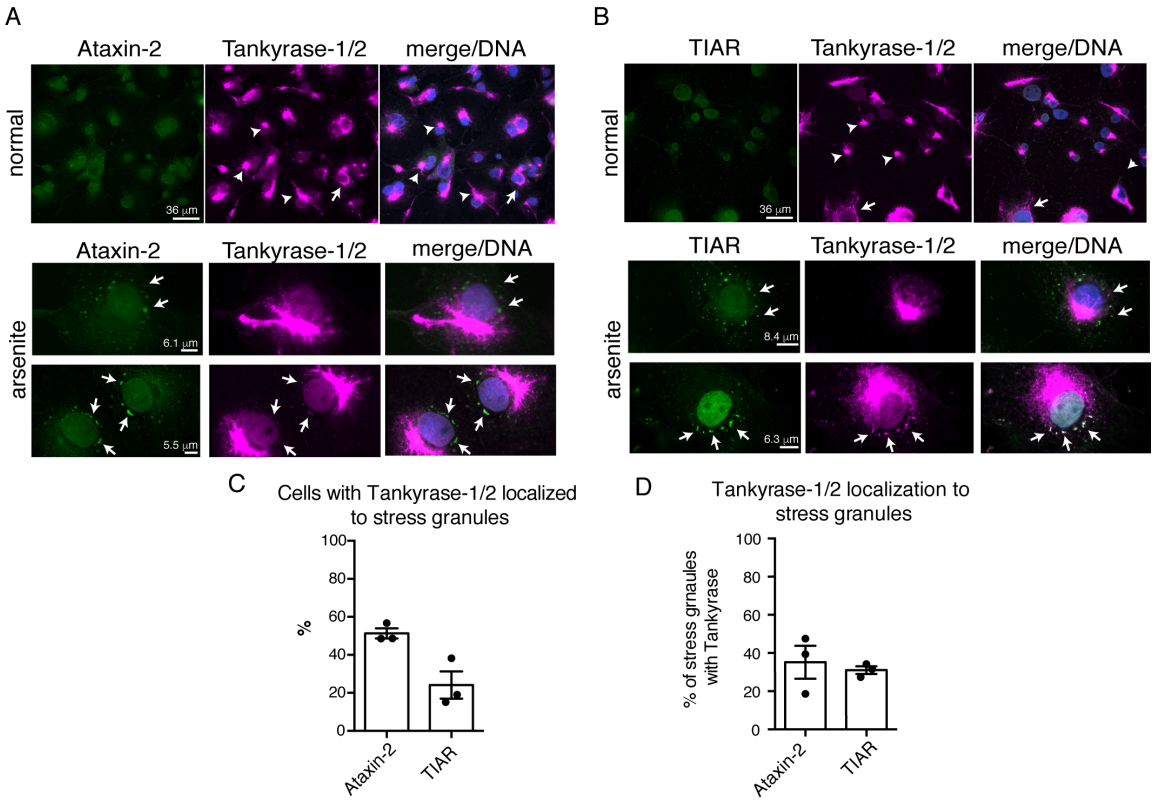

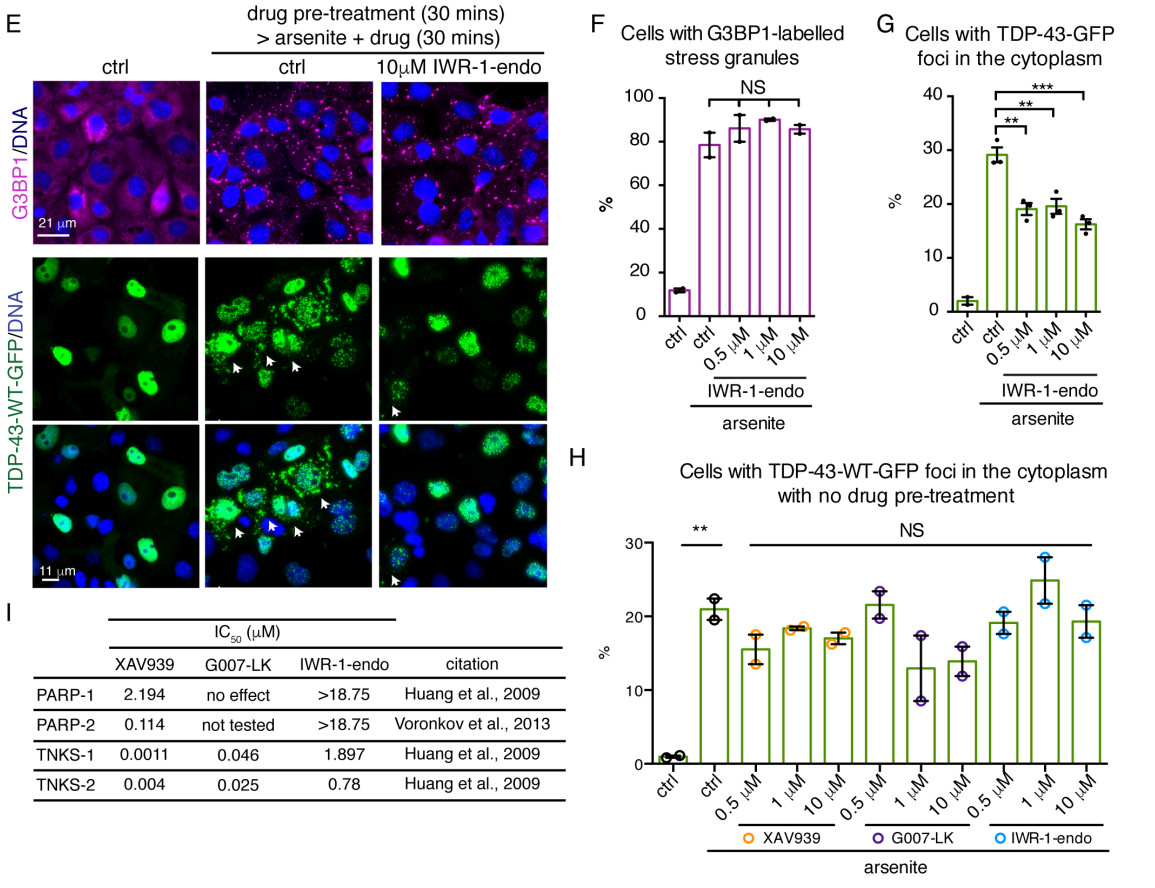

I

	IC_{50} (μM)			
	XAV939	G007-LK	IWR-1-endo	citation
PARP-1	2.194	no effect	>18.75	Huang et al., 2009
PARP-2	0.114	not tested	>18.75	Voronkov et al., 2013
TNKS-1	0.0011	0.046	1.897	Huang et al., 2009
TNKS-2	0.004	0.025	0.78	Huang et al., 2009

Figure S7 (related to Figure 7): Small-molecule inhibitors of Tankyrase-1/2 reduces stress-induced TDP-43 foci without altering the percentage of cells with G3BP1-labelled stress granule formation.

(A) Tankyrase-1/2 and Ataxin-2 immunolocalization in mammalian cells under normal and stress conditions. Arrows in the top panel indicate immunostaining of the nuclear periphery, arrowheads in the top panel indicate example cells with cytoplasmic Tankyrase-1/2, arrows in the middle panel indicate Tankyrase-1/2-negative stress granules and arrows in the lower panel indicate Tankyrase-1/2-positive stress granules. Cells were extracted with 0.5% Triton-X100 for 30 sec prior to fixation in paraformaldehyde, then immunostained for Ataxin-2 and Tankyrase-1/2, and counterstained with Hoescht.

(B) Tankyrase-1/2 and TIAR immunolocalization in mammalian cells under normal and stress conditions. Arrow in the top panel indicate immunostaining of the nuclear periphery, arrowheads in the top panel indicate example cells with cytoplasmic Tankyrase-1/2, arrows in the middle panel indicate Tankyrase-1/2-negative stress granules and arrows in the lower panel indicate Tankyrase-1/2-positive stress granules. Cells were extracted with 0.5% Triton-X100 for 30 sec prior to fixation in paraformaldehyde, then immunostained for TIAR and Tankyrase-1/2, and counterstained with Hoescht.

(C) Cells were quantified for the presence of Tankyrase-1/2 labelling of Ataxin-2 and TIAR labelled stress granules. Cells with one or more Tankyrase-1/2 containing stress granules were counted. The graph represents the mean (± SEM) of three independent experiments.

(D) Ataxin-2 and TIAR-labelled stress granules were quantified for the presence of Tankyrase-1/2 labeling of stress granules. The graph represents the mean (± SEM) of three independent experiments

(E) Cells expressing TDP-43-WT-GFP were either left untreated or treated with 0.5 mM sodium arsenite (30 min) either in the absence of or presence of the Tankyrase-1/2 inhibitor (IWR-1-endo). Cells were pretreated with the indicated amount of inhibitor for 30 min prior to stress. Cells were immunostained for G3BP1 and counterstained with Hoescht. Arrows indicate cells with cytoplasmic TDP-43-WT-GFP foci. Ctrl: control.

(F) Cells were quantified for the presence of G3BP1-labeleld stress granules. The graph represents the mean (± SEM) from two independent experiments, a one-way ANOVA ($p < 0.0001$) and Tukey's test was used to test for significance. NS: not significant.

(G) Cells were quantified for the presence of cytoplasmic TDP-43-GFP foci. The mean (± SEM) from three independent experiments is presented. A one-way ANOVA ($p < 0.0001$) followed by Tukey's test was used to test for significance. Asterisks: significant pairs.

(H) The Tankyrase-1/2 inhibitors were tested for an effect on the formation of TDP-43-GFP foci in the cytoplasm without a 30-min pre-treatment prior to the onset of arsenite treatment. The graph represents the mean of two independent experiments. A one-way ANOVA followed by a Tukey's test revealed that there was no significant difference in the control (ctrl) treated cells compared to drug treated cells. These data indicate that pre-treating the cells with inhibitor is necessary to reduce the formation of stress-induced TDP-43 foci in the cytoplasm. Asterisk: significant pair and NS: not significant.

(I) The reported IC_{50} of XAV939, G007-LK and IWR-1-endo (Huang et al., 2009; Voronkov et al., 2013).

Asterisks:

**: $p < 0.01$ and ***: $p < 0.001$.